Editors' Suggestion

Nematic superconductivity in twisted bilayer graphene

Dmitry V. Chichinadze, Laura Classen, and Andrey V. Chubukov
School of Physics and Astronomy, University of Minnesota, Minneapolis, Minnesota 55455, USA

(Received 16 October 2019; accepted 4 June 2020; published 26 June 2020)

Twisted bilayer graphene displays insulating and superconducting phases caused by exceptional flattening of its lowest energy bands. Superconductivity with highest T_c appears near half filling of the valence band ($n \approx -2$). The data show that in the large part of the superconducting dome near $n = -2$, threefold lattice rotation symmetry is broken in the superconducting phase, i.e., a superconductor is also a nematic. We perform a comprehensive analysis of superconductivity in twisted-bilayer graphene within an itinerant approach and present a mechanism for nematic superconductivity. We take as an input the fact that at dopings, where superconductivity has been observed, the Fermi energy lies in the vicinity of twist-induced Van Hove singularities in the density of states. We argue that the low-energy physics can be properly described by patch models with either six or twelve Van Hove points. We obtain pairing interactions for the patch models in terms of parameters of the microscopic model for the flat bands, which contains both local and twist-induced nonlocal interactions. We show that the latter give rise to attraction in different superconducting channels. For six Van Hove points, there is just one attractive d-wave channel, and we find chiral $d \pm id$ superconducting order, which breaks time-reversal symmetry but leaves the lattice rotation symmetry intact. For twelve Van Hove points, we find two attractive channels, g and i waves, with almost equal coupling constants. We show that both order parameters are nonzero in the ground state and explicitly demonstrate that in this co-existence state the threefold lattice rotation symmetry is broken, i.e., the superconducting state is also a nematic. We find two possible nematic states, one is time-reversal symmetric, the other additionally breaks time-reversal symmetry. We apply our scenario to twisted bilayer graphene near $n = -2$ and argue that it is applicable also to other systems with two (or more) attractive channels with similar couplings as our reasoning for a nematic superconductivity is based on generic symmetry considerations.

DOI: 10.1103/PhysRevB.101.224513

I. INTRODUCTION

Twisted hexagonal heterostructures recently joined the family of condensed matter systems which display superconductivity with a yet unsettled pairing mechanism. Superconductivity (SC) has been observed in twisted bilayer graphene [1–4], twisted double-bilayer graphene [5–7], and trilayer graphene on boron nitride [8,9] under various tuning conditions controlled by twist angle, pressure, filling, or external field. This high degree of tunability holds the promise to enlighten the pairing problem from many different angles and thereby improve our understanding of superconductivity in correlated electron systems. Like in several other correlated systems, SC borders insulated phases, in which fermions either get localized by Mott physics or develop a competing order, which gaps excitations near the Fermi surface.

The occurrence of SC and insulating phases is ascribed to an exceptional band flattening, which comes along with a very large hexagonal moiré pattern in real space [10,11]. The small bandwidth of the resulting isolated flat band increases the relative strength of both electron-electron [12–15] and electron-phonon [16,17] interaction and promotes correlation effects [18]. In twisted bilayer graphene (TBG), insulating and superconducting phases have been induced by adjusting the band flatness either by changing the twist angle between the two graphene layers to the so-called magic angle [11] close to 1.1° or upon applying pressure in the vicinity of the magic angle [1–4]. The most prominent insulating states occur near half filling of either conduction or valence bands at the density of two electrons or two holes per moiré unit cell (near $n = \pm 2$ in the classification where $n = 4$ corresponds to fully occupied and $n = -4$ to empty flat bands). Insulating states have also been reported near other integer fillings [3,4]. Similarly, the SC state with the highest critical temperature $T_c \sim 3$ K [4] was detected close to half filling of the valence band ($n = -2$). Further superconducting states with $T_c \leqslant 0.65$ K have been found near the half-filled conduction band and in between other integer fillings. The suppression of superconductivity by a small magnetic field points to spin-singlet pairing [1].

The data indicate [19] that TBG with a twist angle near the magic one lies in a regime of moderate coupling, where the ratio of Coulomb interaction (reduced by the large spatial scale of the moiré pattern) and the width of the flat band is of order one (both are in the range of 10–20 meV). Consequently, arguments have been made for both moderate coupling itinerant approach and strong coupling Mott-type approach. Arguments for the strong coupling approach have been rationalized by the fact that insulating states have been detected not only near $n = \pm 2$ but also near other integer fillings $n = \pm 1$ and ± 3. Arguments for an itinerant approach are based on the observations that even the highest superconducting T_c of 3 K is much smaller than the bandwidth and that insulating behavior is rather fragile—it disappears already for small $T \geqslant 10$ K and for small fields $H \leqslant 5$ T, Refs. [2–4]. Within the itinerant approach, insulating states are viewed as competing states

with some type of order in the particle-hole channel, and superconductivity and competing orders are largely based on the notion that close to half filling [19,20] and, possibly, other integer fillings, the chemical potential nearly coincides with twist-induced Van Hove (VH) singularities in the density of states, Ref. [21]. This generally amplifies the effect of interactions both in particle-hole and particle-particle channels [22].

In our study, we analyze superconductivity within an itinerant approach. Earlier studies considered both phonon [17,23–26] and purely electronic pairing mechanisms [27–45]. The works on the electronic mechanism often explored a scenario, where the enhancement of the pairing in the doubly degenerate d-wave channel at densities near the VH singularities leads to chiral $d \pm id$ superconductivity. A similar analysis had been previously performed for a single layer of graphene at high doping [46,47].

The primary goal of our study is to take a new look at superconductivity in the presence of VH singularities near the Fermi level in view of the recent experimental observations that a discrete C_3 rotational symmetry is broken in the superconducting state of hole-doped TBG [48]. The breaking of a lattice rotational symmetry is usually associated with nematic order, and a state in which this symmetry is broken below the superconducting T_c is called nematic superconductor. Nematic superconductivity has been earlier discussed for LiFeAs (Ref. [49]) and doped topological insulator Bi_2Se_3 (Refs. [50–57]). In case of TBG, nematic fluctuations were reported in the STM measurements in the normal state [19,58], but no long range nematic order has been detected. The authors of [48] analyzed the nature of a superconducting dome centered near $n = -2$. The superconducting T_c in this dome is higher than at other dopings, where superconductivity has been detected. They found that for most doping levels within the dome, C_3 symmetry is broken below T_c, and they argued that it is very likely caused by superconductivity. For a sliver of dopings within the dome, C_3 breaking was detected already in the normal state. However, the direction of the nematic order is different at dopings where nematicity is only seen in the superconducting state and where it was detected in the normal state, and also T_c drops when normal state nematicity develops. This indicates that the two nematic orders compete with each other, i.e., the nematicity in the normal state is not the source of the nematic order that emerges below T_c. We take these results as a motivation for our study and analyze a possibility to obtain C_3 breaking only in the superconducting state. Out of superconducting states proposed for TBG, $d \pm id$ superconducting order [32–35,38,39,41,44,45] breaks time-reversal symmetry but preserves C_3 rotational symmetry, and s-wave superconductivity due to phonons also does not break C_3 symmetry. Here, we propose a novel scenario for pairing in TBG, which gives rise to nematic superconductivity. We argue that a combination of the geometry of VH points, which can double in number to twelve, and the form of the effective interaction, which was argued to possess both on-site and nearest-neighbor components [13–15], gives rise to an attraction in two pairing channels. Once both pairing condensates emerge, we argue, based on symmetry, that the system becomes a nematic superconductor. In the classification of the lattice rotation group D_3, appropriate for TBG, one of the attractive channels is the doubly degenerate E channel and the other is the single-component A_2 channel. The d-wave state, discussed in earlier works, belongs to E channel. Based on the number of nodes along the Fermi surface, the SC states that we found here correspond to doubly degenerate "g wave" and "i wave," respectively (each gap component in the E channel changes sign eight times under a 2π rotation around the center of the Brillouin zone, while the gap in the A_2 channel changes sign twelve times under a full rotation). The presence of higher lattice harmonics in the superconducting gap structure of TBG was also discussed in Ref. [59]. We argue that the coupling constants in the two channels are quite close, so in a wide temperature range below T_c the system is in the coexistence state, where both SC orders are present. Taken alone, each of the two states does *not* break C_3 symmetry: The order parameter in the E channel $E_1 \pm iE_2$ (the g-wave analog of $d \pm id$) breaks $U(1)$ phase and Z_2 time-reversal symmetry, and the order parameter in the A_2 channel breaks $U(1)$ phase symmetry. We show that in the coexistence state, C_3 symmetry is broken, along with the overall $U(1)$ phase symmetry. The breaking of C_3 symmetry is due to the presence of special coupling terms in the Landau free energy, which are linear in the A_2 order parameter and cubic in the E order parameter. We found two coexistence states: in one time-reversal symmetry is additionally broken, in the other it is preserved. The time-reversal-symmetric state develops if the special coupling between the two order parameters is sufficiently strong. Otherwise, time reversal is broken in the coexistence state. We show the corresponding phase diagrams in Fig. 1 as a function of a tuning parameter α_T, which determines the nonlocal interaction strength and regulates how close the two different SC states are in energy.

It is instructive to compare our findings with the earlier proposals for nematic superconductivity in TBG. For spin-singlet pairing, earlier works [27,60] focused on the two-component E state, without an admixture of the A_2 state. In this situation, nematic superconductivity can develop if the solution for the gap is nonchiral, $(\Delta_{E_1}, \Delta_{E_2}) = \Delta_E(\cos\gamma, \sin\gamma)$, and the minima of the free energy are at three values of γ. We looked into this possibility but found that for parameters extracted from the microscopic model [13,14,61] that we use, the solution for the E state is the chiral $\Delta_{E_1} \pm i\Delta_{E_2}$, which breaks time-reversal but preserves C_3 lattice rotational symmetry. It was suggested [60] that fluctuation corrections can potentially change the free energy and make the nematic configuration energetically favorable, if the nematic component of density wave fluctuations is large in the normal state. In a similar spirit, it was argued in Ref. [37] that fluctuation-induced nematic superconductivity can develop in the vicinity of a transition into a nematic orbital ferromagnet. We did not analyze fluctuation corrections or preformed nematic phases in our model. Instead, we focus on the superconductivity coming already from the bare interaction. In Ref. [62] nematic superconductivity in the triplet channel has been explored. This work is likely applicable to twisted double-bilayer graphene, where data suggest spin-polarized pairing [6]. In TBG, which we consider, experiments point to spin-singlet pairing [1].

The doubling of the number of VH points as a function of twist angle or pressure, and the difference in the number of VH points in valence and conduction bands has been considered for twisted bilayer graphene in Refs. [30,63] and

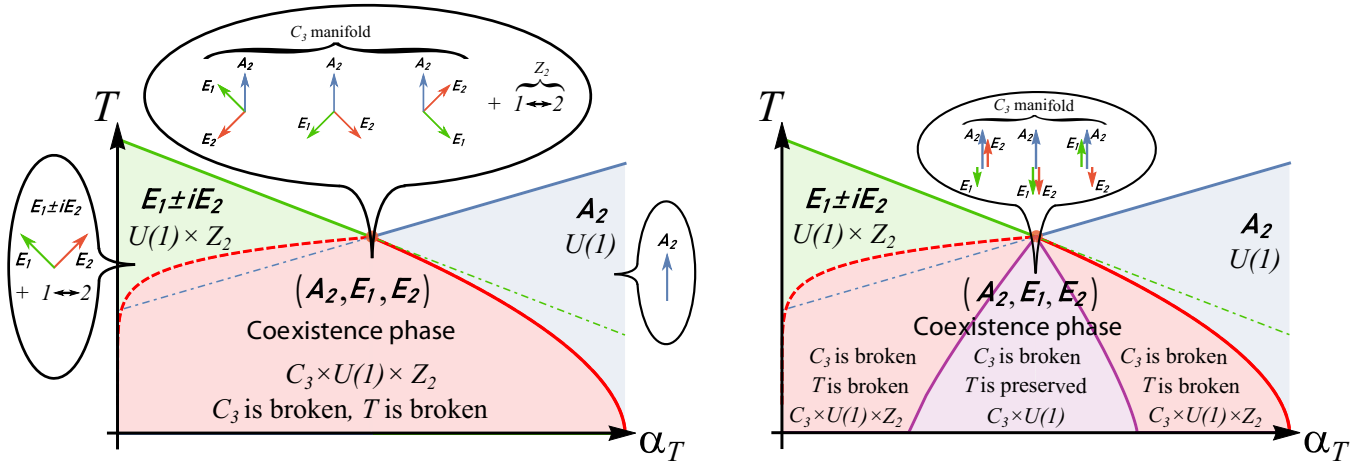

FIG. 1. A schematic phase diagram for the case when the pairing channels with E and A_2 symmetry are nearly degenerate (i.e., the attractive interaction in the two channels has almost the same magnitude). We use the strength of the nonlocal interactions α_T as a parameter to distinguish between the cases when the interaction in one of the channels is stronger than in the other. Immediately below the onset of the pairing, SC develops in one of the two channels, and the gap symmetry is either $g \pm ig$ (E-channel, green shaded region) or i (A_2-channel, blue shaded region); both states are rotationally symmetric. At a lower temperature, a coexistence state develops (red shaded region). Depending on the parameters in the Landau free energy, this state is either type I or type II. State of type I (left panel) evolves continuously between pure A_2 and pure E states. This state breaks C_3 rotational symmetry, i.e., it is a nematic superconductor, and also breaks time-reversal symmetry. For state of type II (right panel), there is an additional intermediate phase inside the coexistence region (purple region). In this intermediate phase, C_3 rotational symmetry is broken, but time-reversal symmetry is preserved. In both panels, the transition between the E state and the co-existence state is first order (red dashed line), and the transition between the co-existence state and the A_2 state is second order (solid red line). The three states in the "bubble" in the middle of each panel are symmetry partners of the C_3 manifold; time-reversal symmetry is realized by exchanging $E_1 \leftrightarrow E_2$. The directions of blue, green, and brown arrows correspond to the phases of A_2, E_1, and E_2 order parameters, $\Delta_i = |\Delta_i| e^{i\phi_i}$, counted from the y axis. For definiteness, we set the A_2 order parameter to be real.

for monolayer jacutingaite in Ref. [64]. In particular, Ref. [30] analyzed Kohn-Luttinger superconductivity within the model with twelve VH points and Hubbard interactions. They found attraction in several channels, with the dominant one being spin-triplet and C_3 symmetric. Our analysis differs from Ref. [30] in two aspects. First, we argue that the nonlocal component of the interaction gives rise to an attraction in more that one channel already at the bare level, and, second, we argue that, to find nematic superconductivity, one needs to move below the highest T_c and analyze the coexistence phase.

The structure of our paper is as follows. In Sec. II we introduce the patch models with six and twelve VH points and extract the model parameters from the underlying microscopic tight-binding model with local and nonlocal interactions. In Sec. III we solve the corresponding linearized gap equation and determine the symmetries of its solutions. We use the result to derive the Landau free energy for spin-singlet superconductivity in TBG in Sec. IV. We analyze the free energy in detail and present possible SC phase diagrams in the end. We conclude in Sec. VI. Several details of the derivations are presented in the Supplemental Material [65]. Before we proceed, we present a brief summary of our results.

Summary of the results

We use as an input for our study the effective tight-binding model for the flat bands, introduced in Refs. [13,14,61,66]. The precise form of the dispersion will not be essential to our analysis, as we will only need the very fact that the dispersion possesses VH points. We argue that the number of VH points is six, if the dispersion is such that VH points are located along one of the high-symmetry directions in the Brillouin zone and twelve if VH points are located away from high-symmetry directions (see Fig. 4). We consider fermionic densities at which VH singularities are located near the chemical potential and introduce patch models for fermions in hot regions near the VH points. We study separately the cases of six and twelve VH points. We argue that nematic superconductivity emerges for the case of twelve VH points. We include all symmetry-allowed interactions between hot fermions and extract their values from the microscopic model of Ref. [13]. In this model the interaction term has both local (Hubbard) and nonlocal (nearest-neighbor) components, with comparable strength.

Within the patch models, we solve for spin-singlet pairing in various channels. The pairing states can be classified according to irreducible representations of the point group D_3, appropriate for TBG. This point group has three irreducible representations: two one-dimensional representations A_1, A_2 and one two-dimensional representation E [67]. We find that the interaction in some pairing channels is attractive, because of the nonlocal component.

For the six-patch model, we find that the E channel (d wave) is attractive, while the A_1 channel (s wave) is repulsive. The A_2 channel (f wave) does not contribute to spin-singlet pairing. This is in accordance with earlier studies of the six-patch model for TBG [28] and single-layer graphene [46]. The corresponding SC order parameter can be represented by a vector $\mathbf{\Delta}^E_{6p}$ with a number of components equal to the number of patches. Because the E channel is two-dimensional, there are two independent order-parameter vectors $\mathbf{\Delta}^{E_1}_{6p}$ and $\mathbf{\Delta}^{E_2}_{6p}$,

and the full SC gap is a linear combination $\Delta_{6p}^{SC} = \Delta_{E_1}\mathbf{\Delta}_{6p}^{E_1} + \Delta_{E_2}\mathbf{\Delta}_{6p}^{E_2}$. The type of the superconducting order depends on which linear combination minimizes the free energy. It is determined by the sign of the coupling term between Δ_{E_1} and Δ_{E_2}: $\beta_2|\Delta_{E_1}^2 + \Delta_{E_2}^2|^2$. When $\beta_2 > 0$, a chiral $\Delta_{E_1} \pm i\Delta_{E_2}$ state develops, when $\beta_2 < 0$ nematic SC develops with $(\Delta_{E_1}, \Delta_{E_2}) = \Delta_E(\cos\gamma, \sin\gamma)$. For the microscopic model that we use for TBG, we find $\beta_2 > 0$, i.e. the SC state is chiral $\Delta_{E_1} \pm i\Delta_{E_2}$. This order breaks time-reversal symmetry but preserves lattice rotational symmetry (the gap amplitude is the same at all six VH points).

For the twelve patch model, we find that two channels, E and A_2, are attractive with nearly equal coupling constants. Analogously to the six-patch case, the corresponding order parameters are twelve-component vectors, which can be expressed as $\Delta_{12,E}^{SC} = \Delta_{E_1}\mathbf{\Delta}_{12p}^{E_1} + \Delta_{E_2}\mathbf{\Delta}_{12p}^{E_2}$ and $\Delta_{12,A_2}^{SC} = \Delta_{A2}\mathbf{\Delta}_{12p}^{A_2}$. The minimization of the free energy for the E state taken alone again yields the chiral $\Delta_{E_1} \pm i\Delta_{E_2}$ state that breaks time-reversal symmetry but preserves C_3 lattice rotation symmetry. The A_2 state with a single gap amplitude Δ_{A_2} preserves both time-reversal and lattice rotation symmetries. However, we show that new states emerge at low temperatures, when both E and A_2 gaps are nonzero. To study the order parameter in the coexistence state, we derive the Landau functional $F[\Delta_{E_1}, \Delta_{E_2}, \Delta_{A2}]$. The functional, taken to quartic order in Δ_i, contains regular mixed terms, quadratic in $\Delta_{E_1}, \Delta_{E_2}$, and in Δ_{A_2}: $\gamma_1(|\Delta_{E_1}|^2 + |\Delta_{E_2}|^2)|\Delta_{A_2}|^2 + \gamma_2((\Delta_{E_1}^2 + \Delta_{E_2}^2)\bar{\Delta}_{A_2}^2 + \text{c.c.})$, and the asymmetric term $\delta\bar{\Delta}_{A_2}[(\Delta_{E_1} - i\Delta_{E_2})^2(\bar{\Delta}_{E_1} - i\bar{\Delta}_{E_2}) + (\Delta_{E_1} + i\Delta_{E_2})^2(\bar{\Delta}_{E_1} + i\bar{\Delta}_{E_2})] + \text{c.c.}$ The coefficients $\gamma_{1,2}$, β_2, and δ are all expressed via the parameters of the underlying microscopic model. The asymmetric term is special in the sense that it is linear in Δ_{A_2} and qubic in $\Delta_{E_{1,2}}$, yet it is invariant under all symmetry transformations from the D_3 space group on the hexagonal lattice, as well as under time-reversal and $U(1)$ gauge transformations. We argue that because of this term, the order parameter in the coexistence state breaks C_3 lattice rotational symmetry.

To illustrate the root of the C_3 breaking, we analyze separately the special case when the asymmetric term is absent, and the generic, proper case when it is present. In the special case, we found that there are two coexistence states. Both are highly degenerate, with order parameter manifold $U(1) \times U(1) \times Z_2$ in one phase and $U(1) \times U(1)$ in the other. The presence of two $U(1)$'s implies that there is an additional continuous degeneracy besides the conventional $U(1)$ overall phase degeneracy. The extra Z_2 in one phase is associated with time reversal. In the other phase, time-reversal operation is a part of the extra $U(1)$ symmetry. In a generic case, when δ is finite, we find that the additional $U(1)$ gets discretized. For small δ, we find that there exists a single coexistence phase with order parameter manifold $U(1) \times C_3 \times Z_2$, where $U(1)$ is phase degeneracy, C_3 is a discrete symmetry with respect to lattice rotations, and Z_2 is associated with time reversal. The superconducting order breaks all three symmetries, including C_3 symmetry of lattice rotations. This implies that the coexistence state is a nematic superconductor. For larger δ we find that there appears a region within the coexistence state, where the order parameter manifold is $U(1) \times C_3$. A SC order in this range is again nematic, but it does not break time-reversal symmetry. For the parameters of the microscopic model of Refs. [13,14,61], the value of δ is close to the boundary where the state with broken C_3 and unbroken time-reversal symmetry develops. We therefore cannot rigorously argue for or against time-reversal breaking in the superconducting state of TBG. Still, we emphasize that for any $\delta > 0$, the SC state in our twelve-patch model breaks C_3 lattice rotational symmetry, i.e., the SC state is also a nematic state. This is consistent with the experiments, which near $n = -2$ found a twofold anisotropy of resistivity in the vortex state as a function of the direction of the applied magnetic field [48,68].

II. EFFECTIVE PATCH MODELS FROM TIGHT BINDING

A. Fermiology of twisted bilayer graphene

While a brute-force microscopic description of TBG is obstructed by the huge unit cells of the moiré superlattice, low-energy continuum [11,20,69–76] and tight-binding [10,77–80] models that couple both layers have been very successful in analyzing the electronic properties of TBG—including the theoretical prediction of flat bands itself [11,69,72,78]. More recent works derived effective tight-binding models for the superlattice based on localized Wannier states exclusively for the isolated flat bands [12,14,61,66]. These Wannier states have a three-peak structure centered around sites of the honeycomb lattices, which is dual to the triangular moiré lattice where the local charge density is concentrated. Such a structure gives rise to hopping between further neighbors. To write down a tight-binding model exclusively for TBG flat bands one has to overcome Wannier obstructions [81,82]. The obstruction occurs if one implements symmetries at incommensurate twist angles. These symmetries are not exact but are assumed to emerge. To avoid the obstruction and construct a tight-binding model for the flat bands only, one can either consider commensurate structures near the magic angle with well-defined bands [66], or sacrifice one of the approximate symmetries [14]. The resulting model (the one we use below) then has a threefold symmetry instead of a sixfold one.

In this work, we employ the model for the dispersion proposed by Yuan and Fu [61] (see also Ref. [14]). We start from writing down the tight-binding Hamiltonian for the moiré superlattice in real space in terms of Wannier states

$$H_{TB} = H_{TB}^{(0)} + H_{TB}^{(1)} \tag{1}$$

$$H_{TB}^{(0)} = -\sum_i \mu \mathbf{c}_i^\dagger \mathbf{c}_i + \sum_{\langle ij\rangle} t_1[\mathbf{c}_i^\dagger \mathbf{c}_j + \text{H.c.}] + \sum_{\langle ij\rangle_5} t_2[\mathbf{c}_i^\dagger \mathbf{c}_j + \text{H.c.}], \tag{2}$$

$$H_{TB}^{(1)} = \sum_{\langle ij\rangle_5} t_3[(\mathbf{c}_i^\dagger \times \mathbf{c}_j)_z + \text{H.c.}]. \tag{3}$$

Here, the sums go over the sites of the honeycomb lattice, which are centered on the AB or BA regions of the moiré pattern in TBG. The operators $\mathbf{c}_i = (c_{i,x}, c_{i,y})^T$ annihilate electrons with p-wave-like orbital index x and y, μ denotes the chemical potential, t_1, t_2 are real hopping amplitudes between nearest- and fifth-nearest-neighbors, and $\langle ij\rangle_5$ denotes fifth-nearest neighbor (see Fig. 2). A fifth-nearest neighbor

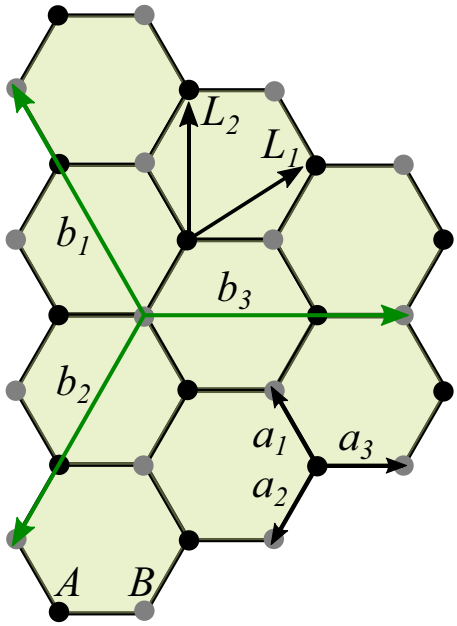

FIG. 2. The moiré honeycomb superlattice and translation vectors relevant for the tight-binding Hamiltonian. Vectors $\boldsymbol{a}_i$ correspond to nearest-neighbor hopping, $\boldsymbol{b}_i$ correspond to hopping between fifth nearest neighbors [denoted by $\langle ij\rangle_5$ in Eq. (1)], and $\boldsymbol{L}_i$ are primitive lattice vectors. Black and gray circles show A and B sublattice sites, respectively.

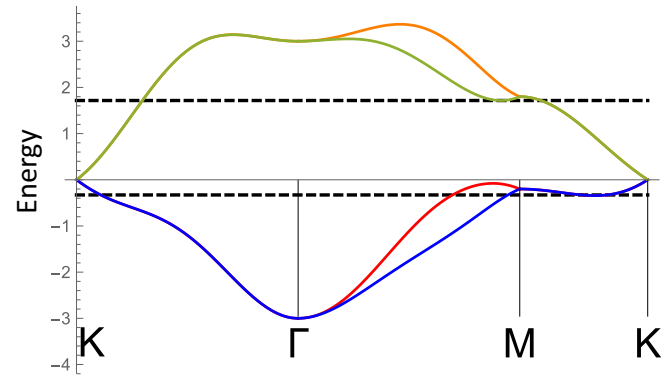

FIG. 3. Band structure for TBG for a particular set of hopping parameters $t_1 = 1, t_2 = -0.1, t_3 = 0.08$. The dashed lines show the positions of VH singularities for electron doping ($\mu \simeq 1.716$) and hole doping ($\mu \simeq -0.329$). The details of the band structure depend on the values of t_i. However, in all cases there are either six or twelve VH singularities.

is equivalent to a second-nearest neighbor within the same sublattice. For simplicity, we suppressed a spin index.

The Hamiltonian $H_{TB}^{(1)}$ possesses an orbital and spin $U(1) \times SU(2)$ symmetry, D_3 space symmetry of the TBG lattice, and is symmetric under time reversal. It yields four spin-degenerate bands with dispersions

$$E_{\pm}^{\pm} = T_d \pm T_{sd2} \pm \sqrt{|T_{sd1}|^2}, \tag{4}$$

where

$$T_d = -\mu + 2t_2(\cos \boldsymbol{b}_1\boldsymbol{k} + \cos \boldsymbol{b}_2\boldsymbol{k} + \cos \boldsymbol{b}_3\boldsymbol{k}), \tag{5}$$

$$T_{sd1} = t_1\left(\exp(ik_x) + 2\exp\left(-i\frac{k_x}{2}\right)\cos\left(\frac{\sqrt{3}k_y}{2}\right)\right), \tag{6}$$

$$T_{sd2} = 2t_3(\sin \boldsymbol{b}_1\boldsymbol{k} + \sin \boldsymbol{b}_2\boldsymbol{k} + \sin \boldsymbol{b}_3\boldsymbol{k}). \tag{7}$$

In Fig. 3 we show the calculated band structure for a particular choice of hopping magnitudes. This band structure is in good agreement with previously published results [11,61,66,73,76]. In particular, it reproduces the splitting of the bands along the ΓM line, obtained in first-principles calculations [2,80,83,84] and effective low-energy models [11,73,76]. The bands are orbitally-polarized in terms of chiral orbitals $c_{\pm} = (c_x \pm ic_y)/\sqrt{2}$. For our purposes, the key feature of the band structure of Eq. (4) and Fig. 3 is that it allows for Lifshitz transitions at both positive and negative energies, and, hence, contains VH points. If such a VH point is a saddle point of the dispersion, the density of states (DOS) is logarithmically singular. The presence of VH points in TBG's band structure has been confirmed experimentally [21]. We will focus on the regions near VH points because the large DOS increases the tendency towards superconductivity. The dashed lines in Fig. 3 mark the values of chemical potential at which saddle-type VH points are located on the Fermi surface. As we will be interested only in the states near the saddle-type VH points, we avoid a subtle issue whether in the presence of all symmetries of TBG, the tight-binding model of Eq. (4), based on localized Wannier states exclusively for the isolated flat bands (Refs. [14,61,66]), is adequate everywhere in the Brillouin zone or if there exist special k points away from VH regions, where one needs to invoke other bands to properly describe excitations [81].

In general, the number of VH singularities in TBG has to be either six or twelve due to the lattice rotation symmetry. We consider both cases because the precise band structure is not known. In particular, the number of VH singularities in conduction and valence bands can differ, even with only a weak particle-hole asymmetry present. The band structure in Fig. 3 is one example, with six VH points upon electron and twelve upon hole doping.

In Fig. 5 we show the evolution of the Fermi surface for either hole or electron doping (negative or positive μ). We see different behavior in the two cases. Upon electron doping, the system reaches a Lifshitz transition with six VH singularities, located away from the Brillouin zone boundary but along high symmetry ΓM directions. Upon hole doping, the first Lifshitz transition creates additional pockets along the ΓM lines but does not give rise to VH singularities. The reason is that VH points in this case are not saddle points but local maxima of the band spectrum. As μ decreases further, the system does undergo a Lifshitz transition accompanied by VH singularities. In this last case, there are twelve VH points in the Brillouin zone, each located away from the Brillouin zone boundary and also away from high symmetry directions. We show the Fermi surfaces with six and twelve VH singularities separately in Fig. 4.

For other values of hopping integrals we found three other scenarios: (a) Lifshitz transitions with six VH singularities for both electron and hole doping, (b) six VH singularities at a Lifshitz transition for hole doping and twelve for electron

doping, and (ii) Lifshitz transitions with twelve VH singularities for both electron and hole doping. The observed electron-hole asymmetry of the superconducting states in TBG [1–4,48] could be a result of different numbers of VH singularities in conduction and valence bands. We show in our analysis below that the superconducting ground state in the case with twelve VH singularities breaks the lattice rotation symmetry, while the one with six does not. The appearance of such a nematic superconducting state has recently been suggested to occur near half filling of the valence band [48]. We also note in passing that as the twelve VH singularities at the Lifshitz transition upon hole doping form six sets of pairs with small separation within a pair, there is the intriguing possibility [63] that for fine-tuned hopping parameters, VH points within each pair merge and create a set of six VH singularities, each leading to a stronger (power-law) divergence of the DOS [85]. We, however, will not study this special case.

B. An effective low-energy patch model

Below we analyze superconductivity near Lifshitz transitions accompanied by singularities in the DOS. For this we focus on states near the VH points and introduce effective patch models with either six or twelve patches. We first expand the energies Eq. (4) around the VH points and approximate the hopping Hamiltonian by

$$H = \sum_{a=1}^{N_p} \sum_{\tau=\pm} \sum_{\sigma=\uparrow,\downarrow} \epsilon_a(\boldsymbol{k}) f^\dagger_{a\tau\sigma}(\boldsymbol{k}) f_{a\tau\sigma}(\boldsymbol{k}), \tag{8}$$

where $f_{a\tau\sigma}(\boldsymbol{k})$ annihilates an electron with momentum $\boldsymbol{k}$ in the vicinity of patch a in band τ with spin σ. The patch index runs through $a = 1 \ldots N_p$ with $N_p = 3$ (6) for the six-patch (twelve-patch) model. The hyperbolic dispersion relations for the different patch points $\epsilon_a(\boldsymbol{k}) = \alpha_a k_x^2 - \beta_a k_y^2$ with $\mathrm{sgn}(\alpha_a) = \mathrm{sgn}(\beta_a)$ are related by D_3 and time-reversal symmetry, inherited from the microscopic Hamiltonian of Eq. (1). Thereby, half of the patch points belong to one of the two bands crossing the Fermi energy at VH doping, while the other half belongs to the other band. The patch points belonging to the same band are related by a threefold rotation symmetry, while the patches from different microscopic bands are related by inversion. We show the location of patches in Figs. 4, 5, and 6.

We next consider all symmetry-allowed coupling terms between fermions in the patches. In general, there are four types of allowed interactions. These are intrapatch and interpatch density-density and exchange interactions. Umklapp processes are not allowed because VH singularities do not appear at momenta connected by a reciprocal lattice vector. A simple bookkeeping analysis shows that there are 6 (18) symmetry-allowed couplings for the six-patch (twelve-patch) model without orbital-mixing terms and 9 (27) when these terms are included. The orbital mixing terms were found to be very small numerically in the microscopic model [13,14], and we do not include them. The most general interacting Hamiltonian for the six-patch model without orbital mixing is [28]

$$\begin{aligned} H^{Int}_{6p} = \sum_{a=1}^{3} \sum_{\tau=\pm} [& u_0 f^\dagger_{a\tau} f_{a\tau} f^\dagger_{a\tau} f_{a\tau} + v_0/2 f^\dagger_{a\tau} f_{a\tau} f^\dagger_{a\bar{\tau}} f_{a\bar{\tau}} + u_1 f^\dagger_{a\tau} f_{a\tau} f^\dagger_{a+1\tau} f_{a+1\tau} + v_1 f^\dagger_{a\tau} f_{a\tau} f^\dagger_{a+1\bar{\tau}} f_{a+1\bar{\tau}} \\ & + j_1 f^\dagger_{a\tau} f_{a+1\tau} f^\dagger_{a+1\tau} f_{a\tau} + (g_1/2 f^\dagger_{a\tau} f_{a+1\tau} f^\dagger_{a\bar{\tau}} f_{a+1\bar{\tau}} + \mathrm{H.c.})]. \end{aligned} \tag{9}$$

We introduced $\bar{\tau} = -\tau$ and a labels half of the patches. We omitted spin indices for simplicity—the spin structure of each term is $\sum_{\sigma,\sigma'} f^\dagger_\sigma f_\sigma f^\dagger_{\sigma'} f_{\sigma'}$.

For the twelve-patch model, the most general interaction Hamiltonian is

$$\begin{aligned} H^{int}_{12p} = \sum_{a=1}^{6} \sum_{\tau=\pm} [& u_0 f^\dagger_{a\tau} f_{a\tau} f^\dagger_{a\tau} f_{a\tau} + v_0/2 f^\dagger_{a\tau} f_{a\tau} f^\dagger_{a\bar{\tau}} f_{a\bar{\tau}} + u_2 f^\dagger_{a\tau} f_{a\tau} f^\dagger_{a+2\tau} f_{a+2\tau} + v_2 f^\dagger_{a\tau} f_{a\tau} f^\dagger_{a+2\bar{\tau}} f_{a+2\bar{\tau}} + u_3 f^\dagger_{a\tau} f_{a\tau} f^\dagger_{a+3\tau} f_{a+3\tau} \\ & + v_3 f^\dagger_{a\tau} f_{a\tau} f^\dagger_{a+3\bar{\tau}} f_{a+3\bar{\tau}} + j_2 f^\dagger_{a\tau} f_{a+2\tau} f^\dagger_{a+2\tau} f_{a\tau} + g_2/2 (f^\dagger_{a\tau} f_{a+2\tau} f^\dagger_{a\bar{\tau}} f_{a+2\bar{\tau}} + \mathrm{H.c.}) + j_3 f^\dagger_{a\tau} f_{a+3\tau} f^\dagger_{a+3\tau} f_{a\tau} \\ & + g_3/2 (f^\dagger_{a\tau} f_{a+3\tau} f^\dagger_{a\bar{\tau}} f_{a+3\bar{\tau}} + \mathrm{H.c.}) + u_{1+} f^\dagger_{a\tau} f_{a\tau} f^\dagger_{a+(-1)^a\tau} f_{a+(-1)^a\tau} + u_{1-} f^\dagger_{a\tau} f_{a\tau} f^\dagger_{a-(-1)^a\tau} f_{a-(-1)^a\tau} \\ & + v_{1+} f^\dagger_{a\tau} f_{a\tau} f^\dagger_{a+(-1)^a\bar{\tau}} f_{a+(-1)^a\bar{\tau}} + v_{1-} f^\dagger_{a\tau} f_{a\tau} f^\dagger_{a-(-1)^a\bar{\tau}} f_{a-(-1)^a\bar{\tau}} + j_{1+} f^\dagger_{a\tau} f_{a+(-1)^a\tau} f^\dagger_{a+(-1)^a\tau} f_{a\tau} \\ & + g_{1+}/2 (f^\dagger_{a\tau} f_{a+(-1)^a\tau} f^\dagger_{a\bar{\tau}} f_{a+(-1)^a\bar{\tau}} + \mathrm{H.c.}) + j_{1-} f^\dagger_{a\tau} f_{a-(-1)^a\tau} f^\dagger_{a-(-1)^a\tau} f_{a\tau} + g_{1-}/2 (f^\dagger_{a\tau} f_{a-(-1)^a\tau} f^\dagger_{a\bar{\tau}} f_{a-(-1)^a\bar{\tau}} + \mathrm{H.c.})] \end{aligned} \tag{10}$$

with the patch index being defined modulo 6.

Below, we will need the subset of interactions relevant to pairing, which are between fermions with opposite momenta. In our model these fermions belong to different bands. The pairing interactions then only involve fermions with patch indices (a, τ) and $(a, \bar{\tau})$ (see Fig. 6). This reduces the number of interaction terms relevant for SC to two, v_0, g_1, for the six-patch model and to five, $v_0, g_2, g_3, g_{1+}, g_{1-}$, for the twelve-patch model. We sketch the interactions which will be important for the pairing problem in Fig. 6.

To estimate the values of the couplings, we need to compare Eqs. (9) and (10) with the corresponding interaction terms in the microscopic model. A typical approximation for the four-fermion interaction term for a system with screened Coulomb interaction is to keep it local, i.e., approximate the interaction by the on-site Hubbard density-density interaction.

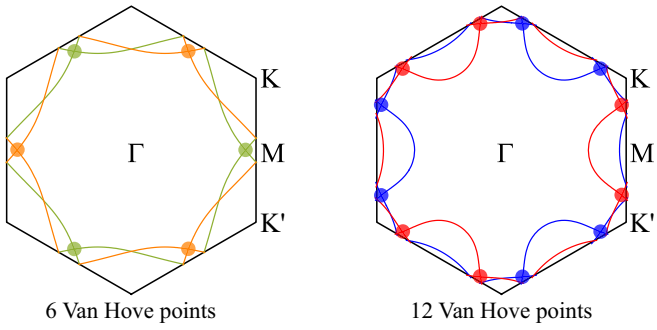

FIG. 4. Fermi surfaces for the two bands (shown by different colors) for $\mu = 1.716$ (left) and $\mu = -0.329$ (right). Circles indicate the positions of VH singularities. For $\mu \simeq 1.716$ (electron doping) there are six VH singularities, located along ΓM and symmetry-related directions in the Brillouin zone. For $\mu \simeq -0.329$ (hole doping) there are twelve VH singularities; neither is located along a high-symmetry direction.

The case of TBG was argued to be different, because there is substantial overlap between Wannier states localized at neighboring sites [13,14]. This peculiar property leads to a new form of the interaction Hamiltonian [13,14], in which local density-density interactions and terms describing assisted nearest neighbor hopping are of the same order and have to be considered on equal grounds. We follow Kang and Vafek [13] and write the interaction Hamiltonian in real space as

$$H_{\text{int}} = V_0 \sum_{\mathbf{R}} \left(\sum_{o=x,y} \sum_{\sigma=\uparrow,\downarrow} O_{o,\sigma}(\mathbf{R}) \right)^2, \tag{11}$$

where

$$O_{o,\sigma}(\mathbf{R}) = \tfrac{1}{3} Q_{o,\sigma}(\mathbf{R}) + \alpha_T T_{o,\sigma}(\mathbf{R}), \tag{12}$$

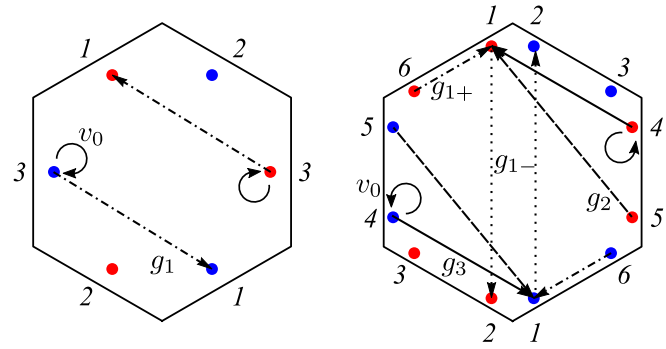

FIG. 6. Sketch of the interactions in six-patch and twelve-patch models. Blue and red dots mark patches around VH points. We show only the interactions relevant for superconductivity.

$$Q_{o,\sigma}(\mathbf{R}) = \sum_{n=1}^{3} (c^{\dagger}_{o\sigma A}(\mathbf{R}+\boldsymbol{a}_n) c_{o\sigma A}(\mathbf{R}+\boldsymbol{a}_n) + c^{\dagger}_{o\sigma B}(\mathbf{R}-\boldsymbol{a}_n) c_{o\sigma B}(\mathbf{R}-\boldsymbol{a}_n)), \tag{13}$$

$$T_{o,\sigma}(\mathbf{R}) = \sum_{n=1}^{3} (c^{\dagger}_{o\sigma B}(\mathbf{R}-\boldsymbol{a}_n) c_{o\sigma A}(\mathbf{R}+\boldsymbol{a}_n) - c^{\dagger}_{o\sigma A}(\mathbf{R}+\boldsymbol{a}_{n+1}) c_{o\sigma B}(\mathbf{R}-\boldsymbol{a}_n) + \text{H.c.}). \tag{14}$$

Here, $\mathbf{R}$ runs over the centers of the honeycomb lattice corresponding to the triangular moiré pattern, A, B denote the sublattice indexes, $\boldsymbol{a}_n$ are three translation vectors of the honeycomb sites (see Fig. 2), and o is the Wannier orbital index, inherited from the original valley degrees of freedom. There are three types of interaction terms: QQ, TQ, QT, and TT terms. The QQ term describes local (Hubbard) density-density interactions within a single honeycomb, the TQ, QT terms

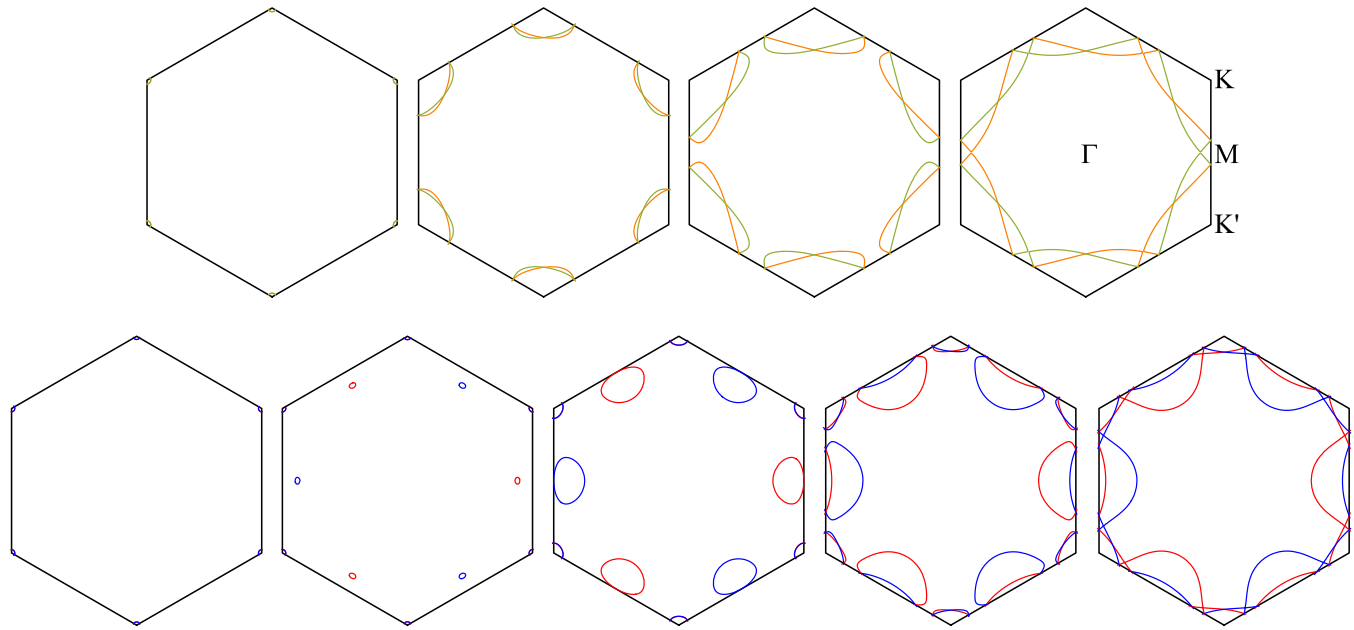

FIG. 5. Evolution of the Fermi surfaces with doping for the same hopping parameters as in Fig. 3. Top: evolution upon electron doping from charge neutrality (Dirac) point on the left to VH doping on the right. Bottom: same evolution upon hole doping.

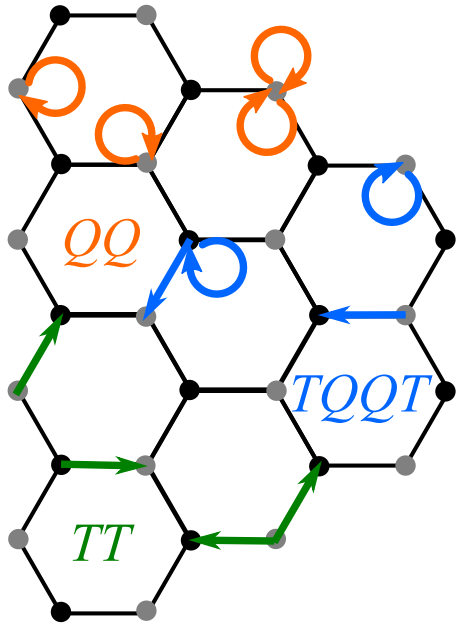

FIG. 7. Graphic representation of three types of interactions in the Hamiltonian of Eq. (11). QQ (orange) are density-density interactions, TQ and QT (blue) describe processes, in which an electron interacts with a local density while hopping to a neighboring site, and TT (green) describes pair hopping processes.

describe the processes, in which an electron interacts with a local density while hopping to a neighboring site, and the TT term describes the pair-hopping processes, in which electrons interact with each other, while hopping to a neighboring site (see Fig. 7). In momentum space, $H_{\rm int}$ becomes

$$\begin{aligned} H_{\rm int} = & \sum_{k,q,k',q'} \sum_{\sigma,\sigma',o,o'} \delta(k-q+k'-q') \\ & \times \Big[\frac{1}{9} \sum_{v,v'} F_{vv'v'v} c^\dagger_{o\sigma vk} c^\dagger_{o'\sigma' v'k'} c_{o'\sigma' v'q'} c_{o\sigma vq} \\ & + \frac{\alpha_T}{3} \sum_{v \neq v'} (F_{vvvv'} c^\dagger_{o\sigma vk} c^\dagger_{o'\sigma' vk'} c_{o'\sigma' vq'} c_{o\sigma v'q} \\ & + F_{vvv'v} c^\dagger_{o\sigma vk} c^\dagger_{o'\sigma' v'k'} c_{o'\sigma' v'q'} c_{o\sigma vq} \\ & + F_{vv'vv} c^\dagger_{o\sigma vk} c^\dagger_{o'\sigma' v'k'} c_{o'\sigma' vq'} c_{o\sigma vq} \\ & + F_{v'vvv} c^\dagger_{o\sigma v'k} c^\dagger_{o'\sigma' vk'} c_{o'\sigma' vq'} c_{o\sigma vq}) \\ & + \alpha_T^2 \sum_{v \neq v'} (F_{vv'vv'} c^\dagger_{o\sigma vk} c^\dagger_{o'\sigma' v'k'} c_{o'\sigma' vq'} c_{o\sigma v'q} \\ & + F_{vvv'v'} c^\dagger_{o\sigma vk} c^\dagger_{o'\sigma' vk'} c_{o'\sigma' v'q'} c_{o\sigma v'q}) \Big], \end{aligned} \tag{15}$$

where v, v' label the sublattice indexes A and B, $F_{vv'v''v'''}$ are coupling functions, which we present in Supplemental Material, and α_T measures the strength of nonlocal interactions (the QQ, TQ, QT, and TT terms are $O(1)$, $O(\alpha_T)$ and $O(\alpha_T^2)$ terms, respectively). Kang and Vafek estimated α_T to be around $1/4$. We will use α_T as a parameter but keep it close to $1/4$.

We next transform $H_{\rm int}$ to the band basis and project it onto the patches around VH points. We show the details in the Supplemental Material and here present the results. For the interactions relevant to SC, we obtain, in units of V_0 from Eq. (11),

$$v_0 = 1 \quad g_1 = 0.1 + 0.92\alpha_T^2 \tag{16}$$

for the six-patch model and

$$\begin{aligned} & v_0 = 1 \quad g_2 = 0.193 + 0.053\alpha_T^2 \quad g_3 = 0.021 + 1.51\alpha_T^2 \\ & g_{1+} = 0.256 + 17.9\alpha_T^2 \quad g_{1-} = 0.057 + 9.02\alpha_T^2 \end{aligned} \tag{17}$$

for the twelve-patch model. Observe that the prefactors of the α_T^2 terms are large numbers.

The interactions in Eqs. (16) and (17) are the bare ones. The true interactions relevant to superconductivity are the effective, fully irreducible ones, which includes all corrections from particle-hole bubbles and also all renormalizations in the particle-particle channel from fermions with energies above the characteristic scale, which is, roughly, the largest of T_c and the Fermi energy at the VH points. The flow of the couplings upon integrating out fermions with higher energies is often described within the renormalization group (RG) approach [86–89]. These renormalizations are particularly relevant when the bare interaction is repulsive in all pairing channels, as renormalizations may overcome the bare repulsion and make the interaction attractive in one or more pairing channels, below certain energies. Physically, these renormalizations make the effective interaction nonlocal, and the growing nonlocal component eventually gives rise to a sign change of the pairing interaction in certain channels. In our case, the bare interaction is already nonlocal, and we show in the next section that it is already attractive in one channel for the six-patch model and in two channels for the twelve-patch model. In this situation, the RG-type renormalization of the bare interaction may affect the magnitudes of the attractive couplings but will unlikely change qualitatively the results obtained with the bare interactions. We therefore proceed without including the RG flow of the couplings. We emphasize that here we only focus on the pairing channel and do not address the issue of competing orders. To study the interplay between superconductivity and competing orders, RG-type calculations are required.

We also note in passing that previous works did apply RG to both six-patch models [28,33,34] and a twelve-patch model [30] for TBG. However, these works considered the cases when the RG flow of the couplings (or, at least, Kohn-Luttinger renormalizations from particle-hole bubbles) is necessary to overcome a bare repulsion and induce an attractive pairing interaction.

III. GAP EQUATION

To study superconductivity, we introduce the gap function as $\Delta_a^{\sigma\tau\sigma'\tau'} = \langle f_{a\tau\sigma} f_{a\tau'\sigma'} \rangle$, where we remind that a labels the patches, and τ and σ are band and spin indices. In the absence of orbital mixing, spin-singlet and spin-triplet channels are degenerate in TBG because direct exchange between patches related by time inversion is absent [28]. A finite orbital mixing splits spin-singlet and triplet channels. Depending on the sign of the orbital mixing term, either spin-singlet or spin-triplet

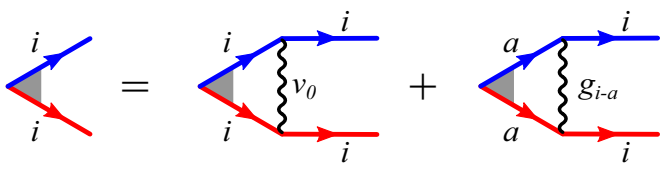

FIG. 8. Diagrammatic representation of a system of coupled gap equations. Gray triangle is a fully renormalized superconducting vertex; red and blue lines are Green's functions of electrons from the two bands. Summation over a is implied.

SC will be favored [28,32]. Experimentally, superconductivity in TBG is destroyed by small magnetic fields [1], which is consistent with spin-singlet pairing. We therefore will focus on spin-singlet pairing. We assume that the orbital mixing term is smaller than the other interaction terms. In this situation, the Cooper pairs with zero total momentum are predominantly made by fermions from different bands, see Figs. 6 and 8. Accordingly, we set $\tau' = \bar{\tau}$ in $\Delta_a^{\sigma\tau\sigma'\tau'}$ and express it as $\Delta_a^{\sigma\tau\sigma'\bar{\tau}} = \Delta_a i\sigma_y$ (Δ_a is the same for the two choices of τ). The matrix gap equation then reduces to a set of three (six) coupled equations for the six-patch (twelve-patch) model:

$$\mathbf{\Delta}_{6p} = -\Pi \begin{pmatrix} v_0 & g_1 & g_1 \\ g_1 & v_0 & g_1 \\ g_1 & g_1 & v_0 \end{pmatrix} \mathbf{\Delta}_{6p}, \tag{18}$$

$$\mathbf{\Delta}_{12p} = -\Pi \begin{pmatrix} v_0 & g_{1-} & g_2 & g_3 & g_2 & g_{1+} \\ g_{1-} & v_0 & g_{1+} & g_2 & g_3 & g_2 \\ g_2 & g_{1+} & v_0 & g_{1-} & g_2 & g_3 \\ g_3 & g_2 & g_{1-} & v_0 & g_{1+} & g_2 \\ g_2 & g_3 & g_2 & g_{1+} & v_0 & g_{1-} \\ g_{1+} & g_2 & g_3 & g_2 & g_{1-} & v_0 \end{pmatrix} \mathbf{\Delta}_{12p}. \tag{19}$$

Here $\mathbf{\Delta}_{6p} = (\Delta, \Delta_2, \Delta_3)^T$, $\mathbf{\Delta}_{12p} = (\Delta, \Delta_2, \Delta_3, \Delta_4, \Delta_5, \Delta_6)^T$, and Π is the particle-particle polarization bubble (the same for all pairs of fermions). Diagonalizing the matrix gap equation, we obtain eigenvalues and eigenfunctions in different pairing channels. We classify the solutions of the gap equation according to the irreducible representations of the point group $D_3 = C_3 \times C_2$, whose elements are rotations along the z axis by $\pm 2\pi/3$ (C_3) and twofold rotations along the y- and symmetry-equivalent axes (C_2), Ref. [67]. The D_3 group has two one-dimensional irreducible representations, called A_1 and A_2, and one two-dimensional representation, called E (the corresponding eigenvalue is doubly degenerate). Each representation contains an infinite set of eigenfunctions; some describe spin-singlet and some spin-triplet order. The generic form of eigenfunctions in A_1 is $\cos(6n\theta_k)$ for spin-singlet pairing ($n = 0, 1, 2..$) and $\sin((6n+3)\theta_k)$ for spin-triplet pairing with the polar angle $\theta_k = \arctan k_y/k_x$ counted from the k_x axis. For A_2, the eigenfunctions are $\cos((6n+3)\theta_k)$ for spin-triplet and $\sin(6n\theta_k)$ for spin-singlet pairing. For E, the eigenfunctions are $(\cos((6n+2)\theta_k), \sin((6n+2)\theta_k))$ and $(\cos((6n+4)\theta_k), \sin((6n+4)\theta_k))$ for spin-singlet pairing and $(\cos((6n+1)\theta_k), \sin((6n+1)\theta_k))$ and $(\cos((6n+5)\theta_k), \sin((6n+5)\theta_k))$ for spin-triplet pairing. The gap equation decouples between different representations but not between different eigenfunctions within the same representation. In a generic case, when all Fermi surface points are relevant to pairing, all partial components get coupled in the gap equation. In patch models, the gap equation simplifies because only a limited number of harmonics is distinguishable. For simplicity, we will use the lowest harmonics to describe our solution of the gap equation.

In our sign convention, a specific channel becomes attractive when the eigenvalue turns from negative to positive. We show below that if we keep only local QQ terms in the interaction (i.e., set $\alpha_T = 0$), all eigenvalues are negative and superconductivity does not occur without additional contributions to the pairing interaction from, e.g., Kohn-Luttinger diagrams. However, once we add nonlocal terms, we find that some channels become attractive once α_T exceeds some critical value, specific to a given channel.

Solving the gap equation for the six-patch model, we find that only one eigenfunction from A_1 and one from E contribute to spin-singlet pairing. To express the corresponding eigenfunctions, we note that the patches are centered along high symmetry directions. In this situation, the polar angles of the patch locations θ_i, $i = 1, 2, 3$, are related by $\theta_2 = \theta_1 - \pi/3$, and $\theta_3 = \theta_1 - 2\pi/3$. We can then write the eigenfunctions as

$$\begin{aligned} \mathbf{\Delta}_{6p}^{A_1} &= (1, 1, 1) \\ \mathbf{\Delta}_{6p}^{E_1} &= (\cos(2\theta_1), \cos(2\theta_1 - 2\pi/3), \cos(2\theta_1 + 2\pi/3)) \\ \mathbf{\Delta}_{6p}^{E_2} &= (\sin(2\theta_1), \sin(2\theta_1 - 2\pi/3), \sin(2\theta_1 + 2\pi/3)). \end{aligned} \tag{20}$$

The eigenfunction in the A_1 representation has the same sign in all patches and is analogous to an s wave. The eigenfunctions in the E representation change sign four times as one makes the full circle along the Fermi surface and in this respect are analogous to d wave.

The eigenvalues in the A_1 and E channels are

$$\lambda_{6p}^{A_1} = -\Pi(v_0 + 2g_1) \tag{21}$$

$$\lambda_{6p}^{E} = -\Pi(v_0 - g_1). \tag{22}$$

Substituting the values of couplings from (16), we obtain

$$\lambda_{6p}^{A_1} = -\Pi V_0\left(1.2 + 1.84\alpha_T^2\right) \tag{23}$$

$$\lambda_{6p}^{E} = -\Pi V_0\left(0.9 - 0.92\alpha_T^2\right). \tag{24}$$

We plot the eigenvalues as functions of α_T in the left panel of Fig. 10. We see that the coupling in the A_1 channel is negative (repulsive) for all values of α_T, but the one in the E channel becomes attractive for $\alpha_T > 0.98$.

For the twelve-patch model, $\theta_{2m+1} = \theta_1 - m\pi/3$, $\theta_2 = \pi - \theta_1$, and $\theta_{2m+2} = \theta_2 - m\pi/3$ (see Fig. 9). This doubles the number of nonequivalent eigenstates and eigenfunctions. The eigenfunctions for spin-singlet pairing are

$$\begin{aligned} \mathbf{\Delta}_{12p}^{A_1} &= (1, 1, 1, 1, 1, 1) \\ \mathbf{\Delta}_{12p}^{A_2} &= (-1, 1, -1, 1, -1, 1) \\ \mathbf{\Delta}_{12p}^{E_1^+} &= (\cos(2\theta_1), \cos(2\theta_1), \cos(2\theta_1 - 2\pi/3), \\ &\quad \cos(2\theta_1 + 2\pi/3), \cos(2\theta_1 + 2\pi/3), \cos(2\theta_1 - 2\pi/3)) \end{aligned}$$

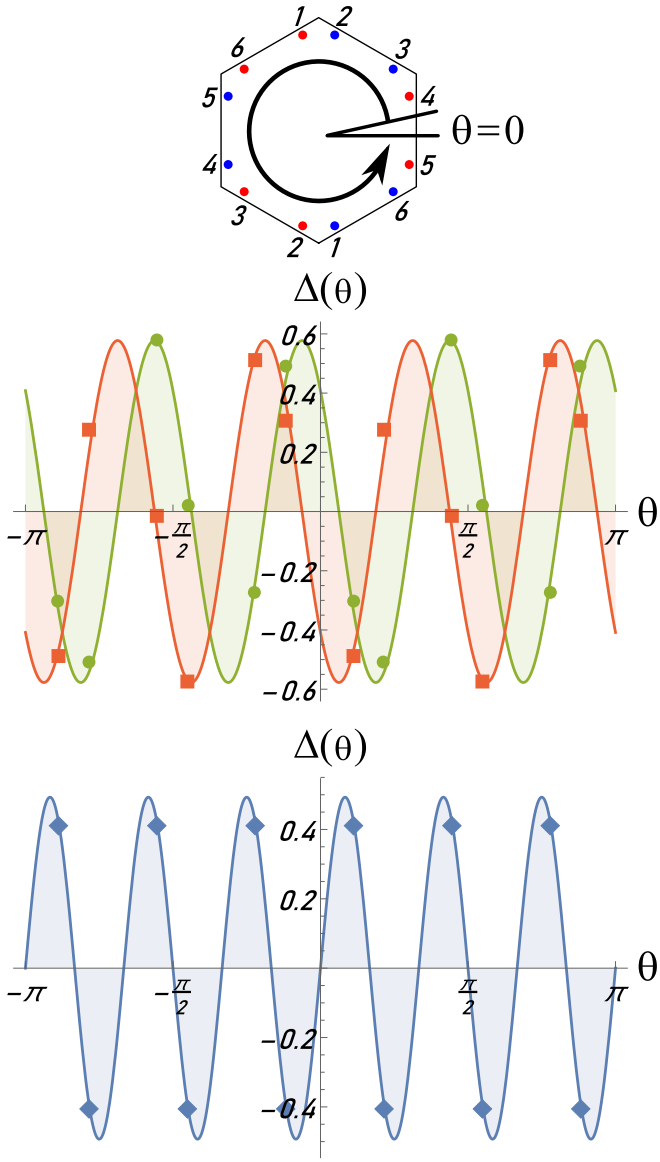

FIG. 9. The eigenfunctions for E and A_2 states in the twelve-patch model. Numbering of VH points is shown on top. Middle: components $\Delta_{12p}^{E_1} = \cos(4\theta_i + 3\pi/4)$ (red) and $\Delta_{12p}^{E_2} = \sin(4\theta_i + 3\pi/4)$ (green). Bottom: $\Delta_{12p}^{A_2} = \sin(6\theta_i)$ (blue). Circles, squares, and diamonds denote the values of gap function at different VH points. Lines are continuous functions of θ, obtained using symmetry reasoning. Viewed as continuous functions, $\Delta_{12p}^{E_1}$ and $\Delta_{12p}^{E_2}$ have eight nodes, and $\Delta_{12p}^{A_2}$ has twelve nodes.

$$\begin{aligned}
\Delta_{12p}^{E_2^+} &= (\sin(2\theta_1), -\sin(2\theta_1), \sin(2\theta_1 - 2\pi/3),\\
&\quad -\sin(2\theta_1 + 2\pi/3), \sin(2\theta_1 + 2\pi/3),\\
&\quad -\sin(2\theta_1 - 2\pi/3))\\
\Delta_{12p}^{E_1^-} &= (\cos(4\theta_1), \cos(4\theta_1), \cos(4\theta_1 + 2\pi/3),\\
&\quad \cos(4\theta_1 - 2\pi/3),\\
&\quad \cos(4\theta_1 - 2\pi/3), \cos(4\theta_1 + 2\pi/3))\\
\Delta_{12p}^{E_2^-} &= (\sin(4\theta_1), -\sin(4\theta_1), \sin(4\theta_1 + 2\pi/3),\\
&\quad -\sin(4\theta_1 - 2\pi/3), \sin(4\theta_1 - 2\pi/3),\\
&\quad -\sin(4\theta_1 + 2\pi/3)).
\end{aligned} \tag{25}$$

With respect to the number of nodes, the A_1 eigenfunction corresponds to s wave. The A_2 eigenfunction is proportional to $\sin(6\theta_k)$ at the patch points and corresponds to i wave (12 nodes along the Fermi surface). Eigenfunctions E^+ and E^- from E correspond to d wave and g wave, respectively (4 nodes and 8 nodes, see Fig. 9). Because the two states with E symmetry have different numbers of nodes, they decouple in the gap equation (this does not hold beyond the patch model).

The eigenvalues in the four decoupled channels are

$$\lambda_{12p}^{A_{1/2}} = -\Pi[v_0 + 2g_2 \pm (g_{1-} + g_{1+} + g_3)], \tag{26}$$

$$\begin{aligned}
\lambda_{12p}^{E^\pm} = -\Pi\big[&v_0 - g_2\\
&\pm \sqrt{g_{1-}^2 + g_{1+}^2 + g_3^2 - g_{1-}g_{1+} - g_{1-}g_3 - g_{1+}g_3}\big].
\end{aligned} \tag{27}$$

Substituting the values for the couplings from (17), we obtain

$$\lambda_{12p}^{A_{1/2}} = -\Pi V_0\big[1.39 + 0.106\alpha_T^2 \pm (0.33 + 28.43\alpha_T^2\big], \tag{28}$$

$$\lambda_{12p}^{E^\pm} = -\Pi V_0\big[0.81 - 0.053\alpha_T^2 \pm \sqrt{0.05 + 5.89\alpha_T^2 + 201.94\alpha_T^4}\big]. \tag{29}$$

We plot the eigenvalues as functions of α_T in the right panel of Fig. 10. We see that $\lambda_{12p}^{A_1}$ and $\lambda_{12p}^{E^+}$ are repulsive for all values of α_T, but $\lambda_{12p}^{A_2}$ and $\lambda_{12p}^{E^-}$ become attractive for $\alpha_T > 0.19$ and 0.21, respectively. Note that the values of α_T needed for attraction are smaller than in the six-patch model and also smaller than the estimate for $\alpha_T \sim 0.23$ presented in Ref. [13]. Furthermore, over some range of $\alpha_T \sim 1/4$, the couplings $\lambda_{12p}^{A_2}$ and $\lambda_{12p}^{E^-}$ are almost identical, i.e., the critical temperatures $T_c^{A_2}$ and T_c^E are approximately the same.

We emphasize that this observation represents a qualitative difference to previous studies of superconductivity within patch models for VH filling in TBG [30,33,90] because in our case no Kohn-Luttinger type corrections (or higher order corrections associated with spin or charge fluctuations) are needed to induce attractive pairing interactions. As a consequence, we anticipate a higher critical temperature than typically expected for Kohn-Luttinger type superconductivity. Fluctuation corrections will increase nonlocal interactions, i.e., shift α_T to a larger value and somewhat increase $T_c^{A_2}$ and T_c^E from already nonzero values.

In the next section we derive the Landau free energy and analyze the SC state below T_c. We show that the near degeneracy between the eigenfunctions in the A_2 and E^- channels leads to a highly nontrivial phase diagram with a large region of the coexistence state, where superconductivity breaks not only the $U(1)$ phase symmetry but also threefold C_3 lattice rotational symmetry, i.e., the SC state is a nematic superconductor. We show that two types of nematic superconductors emerge, depending on system parameters. One additionally breaks time reversal symmetry; the other preserves it.

Before we proceed, we make an adjustment of the E^- state in the 12-patch model for further convenience. Namely, we use the fact that any rotation of the two components of E^- is still an eigenfunction and rotate them by $3\pi/4$. The new

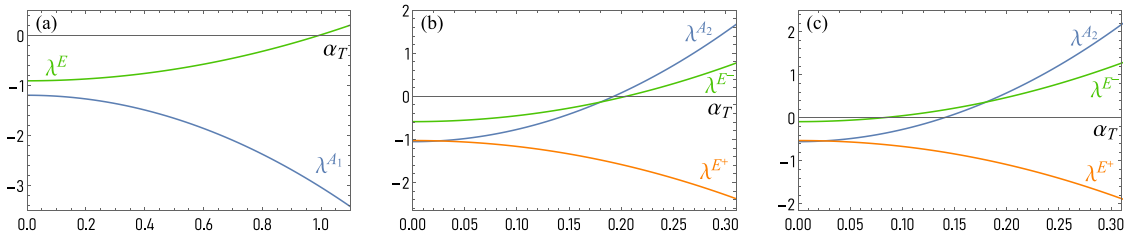

FIG. 10. The eigenvalues for the six-patch model λ^E and λ^{A_1} (a) and for the twelve-patch model, λ^{E^+}, λ^{E^-}, and λ^{A_2} [(b) and (c)], as functions of α_T (λ^{A_1} is irrelevant and not shown). When an eigenvalue turns positive, the interaction in the corresponding pairing channel becomes attractive. For the six patch model, $\lambda^E > 0$ for $\alpha_T > 0.98$. For the twelve patch model, λ^{E^-} and λ^{A_2} become positive when α_T exceeds certain values. Panel (b) is for the interactions, extracted from the microscopic model (see text). For panel (c), we increased exchange interactions by a factor of two. Observe that λ^{E^-} and λ^{A_2} are nearly degenerate over some range of α_T.

components $E_1^- = E_1$ and $E_2^- = E_2$ are

$$\mathbf{\Delta}_{12p}^{E_1} = (\cos(4\theta_1 + 3\pi/4), \ldots, \cos(4\theta_6 + 3\pi/4))$$
$$\mathbf{\Delta}_{12p}^{E_2} = (\sin(4\theta_1 + 3\pi/4), \ldots, \sin(4\theta_6 + 3\pi/4)). \quad (30)$$

With this choice of basis eigenfunctions, $\Delta_{12p}^{E_1}$ and $\Delta_{12p}^{E_2}$ exchange as $\Delta_{12p}^{E_{1,2}} \to -\Delta_{12p}^{E_{2,1}}$ under the twofold rotations around k_y and symmetry related axes.

IV. LANDAU FREE ENERGY AND THE STRUCTURE OF THE SUPERCONDUCTING STATE

We express the gap function in the superconducting state as a linear combination of the eigenfunctions for the attractive pairing components. In the six-patch model we have

$$\Delta_{6p}^{SC} = \Delta_{E_1}\mathbf{\Delta}_{6p}^{E_1} + \Delta_{E_2}\mathbf{\Delta}_{6p}^{E_2}, \quad (31)$$

where Δ_{E_1} and Δ_{E_2} are complex numbers. In the twelve-patch model we have

$$\Delta_{12p}^{SC} = \Delta_{A_2}\mathbf{\Delta}_{12p}^{A_2} + \Delta_{E_1}\mathbf{\Delta}_{12p}^{E_1} + \Delta_{E_2}\mathbf{\Delta}_{12p}^{E_2}, \quad (32)$$

where Δ_{E_1}, Δ_{E_2}, and Δ_{A_2} are complex numbers.

To analyze superconducting ground states, we derive the Landau free energy, $\mathcal{F}_{6p} = \mathcal{F}_{6p}(\Delta_{E_1}, \Delta_{E_2})$ and $\mathcal{F}_{12p} = \mathcal{F}_{12p}(\Delta_{E_1}, \Delta_{E_2}, \Delta_{A_2})$, find their minima, and obtain the magnitudes and phases of Δ_{E_1} and Δ_{E_2} for the six-patch model and of Δ_{A_2}, Δ_{E_1}, and Δ_{E_2} for the twelve-patch model. The functional form of the Landau free energy for each model is determined by D_3 and $U(1)$ symmetries [91], however which superconducting state is realized depends on the parameters of the Landau free energy. We obtain these parameters by applying a Hubbard-Stratonovich decomposition to the underlying fermionic model and integrating out fermions (see Supplemental Material for details).

A. Six-patch model

The Landau functional for the six-patch model to order $\Delta_{E_{1,2}}^4$ has the form

$$\mathcal{F}_{6p} = \alpha_1\left(|\Delta_{E_1}|^2 + |\Delta_{E_2}|^2\right) + \beta_1\left(|\Delta_{E_1}|^2 + |\Delta_{E_2}|^2\right)^2 + \beta_2|\Delta_{E_1}^2 + \Delta_{E_2}^2|^2. \quad (33)$$

As usual, near a superconducting instability, $\alpha_1 \propto (T - T_c)$ and $\beta_1 > 0$. The coupling β_2 can be of any sign, as long as $\beta_1 + \beta_2 > 0$. Minimizing with respect to amplitudes and phases of Δ_{E_1} and Δ_{E_2} we find that for $\beta_2 > 0$, $\mathcal{F}_{6p}$ is minimized by $(\Delta_{E1}, \Delta_{E2}) = \Delta_E e^{i\phi}(1, \pm i)$ (Refs. [46,47]). This state breaks $U(1)$ phase symmetry and additionally breaks Z_2 time-reversal symmetry. For $\beta_2 < 0$, $\mathcal{F}_{6p}$ is minimized by $(\Delta_{E1}, \Delta_{E2}) = \Delta_E(\cos\gamma, \sin\gamma)$, where γ is arbitrary. To fix γ, one needs to include terms of sixth order in $\Delta_{E_{1,2}}$. The relevant sixth-order term is [27,33,46,56,57,91]

$$\mathcal{F}_{6p}^{(6)} = \frac{\lambda}{2}[(\Delta_{E_1} - i\Delta_{E_2})^3(\bar{\Delta}_{E_1} - i\bar{\Delta}_{E_2})^3 + \text{c.c}]. \quad (34)$$

For our six-patch model for electron-doped TBG, we derived β_2 from the underlying microscopic model and found $\beta_2 > 0$, i.e., the SC state is a nodeless chiral superconductor. Such a state, dubbed $d \pm id$, has been found in several earlier studies of superconductivity in TBG [32–35,38,39,41,44,45]. It breaks time-reversal symmetry but does not break C_3 lattice rotational symmetry.

It was argued that nematic fluctuations [27,60] in the normal state (more accurately, nematic components of charge or spin density wave fluctuations) do affect β_2, and if these fluctuations are strong, they can, in principle, reverse the sign of β_2 and convert the SC state in the six-patch model into a nematic SC. We did not analyze the strength of nematic fluctuations in our six-patch model. Instead we show how a nematic SC state can still develop in the twelve-patch model for hole doping, even if $\beta_2 > 0$, due to the presence of another superconducting component.

B. Twelve-patch model

As we demonstrated in Sec. III, there are two attractive pairing channels for the twelve-patch model—one-component A_2 and two-component E channels. Up to fourth order in the gap function, the Landau free energy is

$$\begin{aligned}\mathcal{F}_{12p} = {} & \alpha_1\left(|\Delta_{E_1}|^2 + |\Delta_{E_2}|^2\right) + \alpha_2|\Delta_{A_2}|^2 \\ & + \beta_1\left(|\Delta_{E_1}|^2 + |\Delta_{E_2}|^2\right)^2 + \beta_2|\Delta_{E_1}^2 + \Delta_{E_2}^2|^2 + \beta_3|\Delta_{A_2}|^4 \\ & + \gamma_1\left(|\Delta_{E_1}|^2 + |\Delta_{E_2}|^2\right)|\Delta_{A_2}|^2 \\ & + \gamma_2\left[(\Delta_{E_1}^2 + \Delta_{E_2}^2)\bar{\Delta}_{A_2}^2 + (\bar{\Delta}_{E_1}^2 + \bar{\Delta}_{E_2}^2)\Delta_{A_2}^2\right] \\ & + \delta\left[2\Delta_{E_1}|\Delta_{E_2}|^2 + \bar{\Delta}_{E_1}\Delta_{E_2}^2 - \Delta_{E_1}|\Delta_{E_1}|^2 + 2\Delta_{E_2}|\Delta_{E_1}|^2\right. \\ & \left. + \bar{\Delta}_{E_2}\Delta_{E_1}^2 - \Delta_{E_2}|\Delta_{E_2}|^2\right)\bar{\Delta}_{A_2} + \text{c.c.}\Big], \end{aligned} \quad (35)$$

where the bar on top of Δ means complex conjugation, and $\alpha_1 \propto T - T_c^E$, $\alpha_2 \propto T - T_c^{A_2}$ change sign at the critical

temperatures for the pairing in E and A_2 channels. We find that all prefactors for the fourth-order terms—$\beta_1, \beta_2, \beta_3, \gamma_1, \gamma_2$, and δ—are positive.

Immediately below the largest of T_c^E and $T_c^{A_2}$, the system develops either E or A_2 superconducting order. When T_c^E is larger, we have for the order in the E channel

$$\mathcal{F}_{12p}^E = \alpha_1\left(\left|\Delta_{E_1}\right|^2 + \left|\Delta_{E_2}\right|^2\right) + \beta_1\left(\left|\Delta_{E_1}\right|^2 + \left|\Delta_{E_2}\right|^2\right)^2 + \beta_2\left|\Delta_{E_1}^2 + \Delta_{E_2}^2\right|^2. \tag{36}$$

This $\mathcal{F}_{12p}^E$ has the same form as $\mathcal{F}_{6p}$ in the six-patch model. Like there, we found $\beta_2 > 0$. Then the state immediately below T_c^E is a nodeless SC, which breaks time-reversal symmetry but does not break C_3 lattice rotational symmetry.

When $T_c^{A_2}$ is larger, we have for the order in the A_2 channel

$$\mathcal{F}_{12p}^{A_2} = \alpha_2\Delta_{A_2}^2 + \beta_3\Delta_{A_2}^4. \tag{37}$$

The A_2 order is odd under C_2 rotations, but it does not break C_3 lattice rotation symmetry.

We now consider coexistence states, in which both A_2 and E order parameters are nonzero. We see from Eq. (35) that there are two types of terms in $\mathcal{F}_{12p}$, which contain products of Δ_{A_2} and $\Delta_{E_{1,2}}$. The terms with coefficients γ_1 and γ_2 are "conventional" biquadratic terms, which in a generic case set relative magnitudes and phases of A_2 and E gap components. However, there is the additional term in Eq. (35) with prefactor δ, which is linear in Δ_{A_2} and cubic in Δ_E. Such a term is allowed by all symmetries. Indeed, one can explicitly verify that it is symmetric with respect to an overall $U(1)$ phase rotation and does not change under C_3 and C_2 rotations. For the invariance under C_2, it is essential that our choice of eigenfunctions $\mathbf{\Delta}_{E_1}$ and $\mathbf{\Delta}_{E_2}$ transforms under C_2 as $\mathbf{\Delta}_{E_1} \leftrightarrow -\mathbf{\Delta}_{E_2}$ [see Eq. (30) and discussion after it]. The structure of this δ term is similar to that of the sixth-order term in Eq. (34) of the six-patch model. Indeed, the δ term can be re-expressed as

$$\begin{aligned} -\frac{\delta}{2}\bar{\Delta}_{A_2}\big(\big[&\left(\Delta_{E_1} - i\Delta_{E_2}\right)^2\left(\bar{\Delta}_{E_1} - i\bar{\Delta}_{E_2}\right) \\ &+ \left(\Delta_{E_1} + i\Delta_{E_2}\right)^2\left(\bar{\Delta}_{E_1} + i\bar{\Delta}_{E_2}\right)\big] \\ &- i\big[\left(\Delta_{E_1} - i\Delta_{E_2}\right)^2\left(\bar{\Delta}_{E_1} - i\bar{\Delta}_{E_2}\right) \\ &- \left(\Delta_{E_1} + i\Delta_{E_2}\right)^2\left(\bar{\Delta}_{E_1} + i\bar{\Delta}_{E_2}\right)\big]\big) + \text{c.c.} \end{aligned} \tag{38}$$

We will show that the δ term in the twelve-patch model and the sixth-order term in the six-patch model will play a similar role regarding the breaking of lattice rotation symmetry. We note in passing that the term cubic in one SC order parameter and linear in the other was recently proposed in Ref. [92] in the context of chiral p- and f-wave pairing states on the square lattice, with application to Sr_2RuO_4.

To understand the role played by the δ term, it is instructive to first consider the structure of the coexistence state without this term and then add it. This is what we do next.

1. The structure of the coexistence state for $\delta = 0$

Without loss of generality, we choose the phase of complex Δ_{A_2} to be zero, i.e., set Δ_{A_2} to be real. We parametrize complex Δ_{E_1} and Δ_{E_2} as

$$\begin{pmatrix}\Delta_{E_1}\\ \Delta_{E_2}\end{pmatrix} = \Delta_E e^{i\phi_+}\begin{pmatrix}e^{i\phi_-}\cos\gamma\\ e^{-i\phi_-}\sin\gamma\end{pmatrix}, \tag{39}$$

where $\gamma \in [0, \pi/2]$. Using this parametrization, we rewrite the Landau free energy Eq. (35) with $\delta = 0$ as

$$\begin{aligned}\mathcal{F}_{12p}^{\delta=0} = {}& 2\alpha_1\Delta_E^2 + \alpha_2\Delta_{A_2}^2 + \beta_1\Delta_E^4 + \beta_3\Delta_{A_2}^4 + \gamma_1\Delta_E^2\Delta_{A_2}^2 \\ &+ \tilde{\beta}_2(\cos^2 2\gamma + \sin^2 2\gamma\cos^2 2\phi_-) \\ &+ 2\tilde{\gamma}_2(\cos 2\phi_+\cos 2\phi_- - \sin 2\phi_+\sin 2\phi_-\cos 2\gamma),\end{aligned} \tag{40}$$

where $\tilde{\beta}_2 = \beta_2\Delta_E^4$, $\tilde{\gamma}_2 = \gamma_2\Delta_E^2\Delta_{A_2}^2$. Minimizing the functional, we find two types of solutions, one for $\tilde{\gamma}_2 < \tilde{\beta}_2$, another for $\tilde{\gamma}_2 > \tilde{\beta}_2$. The first solution is realized when the coexistence state emerges out of the E state; the second is when it emerges from the A_2 state.

For $\tilde{\gamma}_2 < \tilde{\beta}_2$ we obtain from minimization

$$\begin{aligned}\cos 2\phi_- &= -\frac{\tilde{\gamma}_2}{\tilde{\beta}_2}\cos 2\phi_+ \\ \cos 2\gamma &= \frac{\tilde{\gamma}_2\sin 2\phi_+}{\tilde{\beta}_2\sin 2\phi_-}.\end{aligned} \tag{41}$$

At $\Delta_{A_2} = 0$, $\tilde{\gamma}_2 = 0$, and Eq. (41) yields $\gamma = \pi/4$ and $\phi_- = \pm\pi/4$, as expected for the pure E state.

Substituting $\cos 2\phi_-$ and $\cos 2\gamma$ from Eq. (41) into the Landau free energy, we find that

$$\begin{aligned}\mathcal{F}_{12p}^{\delta=0} &= 2\alpha_1\Delta_E^2 + \alpha_2\Delta_{A_2}^2 + \beta_1\Delta_E^4 + \beta_3\Delta_{A_2}^4 \\ &\quad + \gamma_1\Delta_E^2\Delta_{A_2}^2 - \frac{\tilde{\gamma}_2^2}{\tilde{\beta}_2} \\ &= 2\alpha_1\Delta_E^2 + \alpha_2\Delta_{A_2}^2 + \beta_1\Delta_E^4 + \beta_3\Delta_{A_2}^4 \\ &\quad + \gamma_1\Delta_E^2\Delta_{A_2}^2 - \frac{\gamma_2^2\Delta_{A_2}^4}{\beta_2}\end{aligned} \tag{42}$$

does not depend on ϕ_+. This implies that the order parameter manifold contains, in addition to $U(1)$ total phase symmetry, another extra $U(1)$, associated with the freedom to rotate the common phase of Δ_{E_1} and Δ_{E_2} with respect to Δ_{A_2}. In addition, Eq. (41) for fixed ϕ_+ allows two solutions (ϕ_-, γ) and $(-\phi_-, \pi/2 - \gamma)$. One solution transforms into the other if we interchange Δ_{E_1} into Δ_{E_2}. The full order parameter manifold is then $U(1)\times U(1)\times Z_2$. One can verify that this Z_2 is associated with time-reversal symmetry.

For $\tilde{\gamma}_2 > \tilde{\beta}_2$, the solution Eq. (41) disappears. The new minima are at

$$\begin{matrix}\phi_+ = 0\\ \phi_- = \pm\pi/2\end{matrix} \quad \text{and} \quad \begin{matrix}\phi_+ = \pm\pi/2\\ \phi_- = 0\end{matrix}. \tag{43}$$

Substituting these solutions into the Landau free energy, we obtain that it does not depend on γ:

$$\begin{aligned}\mathcal{F}_{12p}^{\delta=0} &= 2\alpha_1\Delta_E^2 + \alpha_2\Delta_{A_2}^2 + \beta_1\Delta_E^4 \\ &\quad + \beta_3\Delta_{A_2}^4 + \gamma_1\Delta_E^2\Delta_{A_2}^2 + \tilde{\beta}_2 - 2\tilde{\gamma}_2 \\ &= 2\alpha_1\Delta_E^2 + \alpha_2\Delta_{A_2}^2 + \beta_1\Delta_E^4 + \beta_3\Delta_{A_2}^4 \\ &\quad + \gamma_1\Delta_E^2\Delta_{A_2}^2 + \beta_2\Delta_E^4 - 2\gamma_2\Delta_E^2\Delta_{A_2}^2.\end{aligned} \tag{44}$$

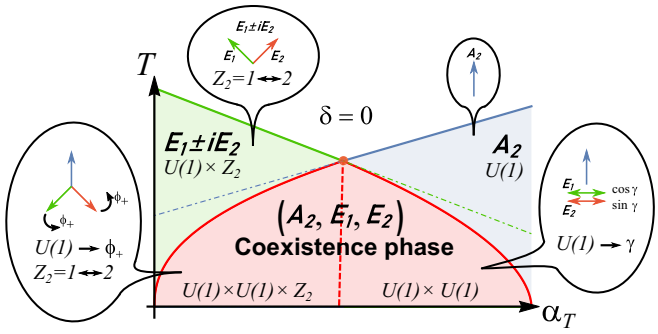

FIG. 11. A schematic phase diagram for the special case $\delta = 0$ in Eq. (35) for the free energy. We use the strength of the nonlocal interactions α_T as tuning parameter. The orange circle marks the point where A_2 and E channels are exactly degenerate. In the green shaded region the superconducting state is pure E ($E_1 \pm iE_2$), in the blue shaded region the SC is pure A_2. In the red shaded region, both $E = (E_1, E_2)$ and A_2 gap components are nonzero. The dashed red line marks a phase transition between two coexistence states with different order parameter manifolds. On the left of this line the manifold is $U(1) \times U(1) \times Z_2$, on the right it is $U(1) \times U(1)$. In both cases, the order parameter manifold contains an additional continuous $U(1)$ symmetry. The insets illustrate symmetry operations. The directions of blue, green, and brown arrows correspond to the phases of A_2, E_1, and E_2 order parameters.

This means that the order parameter manifold again has an additional continuous $U(1)$ symmetry. To obtain the full order parameter manifold in this case, we note that the four solutions in Eq. (43) can be re-expressed as

$$\begin{pmatrix} \Delta_{E_1} \\ \Delta_{E_2} \end{pmatrix} = i\Delta_E \begin{pmatrix} \cos\gamma \\ \sin\gamma \end{pmatrix}, \tag{45}$$

if we allow γ to vary between zero and 2π. This implies that the order parameter manifold for $\tilde{\gamma}_2 > \tilde{\beta}_2$ is $U(1) \times U(1)$. There is no additional Z_2, because the phase of Δ_{E_1} and Δ_{E_2} in (45) is either the same or differs by π, in which case phase reversal does not create a distinct SC state. Put differently, the interchange $\Delta_{E_1} \leftrightarrow \Delta_{E_2}$ can be absorbed into a variation of γ.

We show the phase diagram for $\delta = 0$ and sketches of the gap configurations in Fig. 11 with α_T as a tuning parameter. Along the transition line at $\tilde{\gamma}_2 = \tilde{\beta}_2$, one of the E components vanishes, and the order parameter manifold reduces to $U(1) \times Z_2$.

The existence of the continuous $U(1)$ symmetry in the order parameter manifold is highly unusual. In general, one would expect only one $U(1)$ to be present, associated with the symmetry with respect to rotations of the common phase. We will see below that in the presence of the δ term, the continuous $U(1)$ symmetry is replaced by a discrete C_3 symmetry.

2. *The structure of the coexistence state for nonzero δ*

Next, we consider the full Landau free energy, Eq. (35), with the δ term. We use the same parametrization as in Eq. (39). The full analysis of Eq. (35) is rather cumbersome, but the outcome can be understood by just expanding near the boundaries of the coexistence phase. Near the left boundary, where $\Delta_{A_2} \ll \Delta_E$, we have at $\delta = 0$ $\gamma = \pi/4$ and $\phi_- = \pm\pi/4$. Accordingly, at finite δ, we set $\gamma = \pi/4 + \epsilon_\gamma$ and $\phi_- = \pm(\pi/4 + \epsilon_-)$, where $\epsilon_\gamma, \epsilon_- \sim \delta\Delta_{A_2}/\Delta_E \ll 1$. We will see below that this expansion is valid for $\delta^2 < 2\beta_2\gamma_2$. The solutions with opposite sign of ϕ_- transform into each other under $\Delta_{E_1} \leftrightarrow \Delta_{E_2}$, i.e., the order parameter manifold contains Z_2 associated with time reversal, like for $\delta = 0$.

Substituting this expansion into (35) and minimizing with respect to $\epsilon_\gamma, \epsilon_-$, we obtain to leading order in Δ_{A_2}/Δ_E:

$$\begin{aligned} \epsilon_\gamma &= \frac{\delta}{2\beta_2}\frac{\Delta_{A_2}}{\Delta_E}\sin\phi_+ \\ \epsilon_- &= \frac{\delta}{2\beta_2}\frac{\Delta_{A_2}}{\Delta_E}\cos\phi_+. \end{aligned} \tag{46}$$

Substituting these expressions back into the Landau free energy we obtain

$$\begin{aligned} \mathcal{F}_{12p} = \mathcal{F}_{12p}^{\delta=0} - \frac{\delta^2}{\beta_2}\Delta_E^2\Delta_{A_2}^2 - \delta\frac{2\beta_2\gamma_2 - \delta^2}{\beta_2^2}\cos 3\phi_+\Delta_E\Delta_{A_2}^3 \\ + \delta^2\frac{8\beta_2\gamma_2 - 3\delta^2}{4\beta_2^3}\Delta_{A_2}^4. \end{aligned} \tag{47}$$

We see that the free energy now depends on ϕ_+ via the $\cos 3\phi_+$ term. For $\delta^2 < 2\beta_2\gamma_2$, minimization with respect to ϕ_+ yields three solutions $\phi_+ = (0, 2\pi/3, -2\pi/3)$. We see that the δ term reduces the additional continuous $U(1)$ symmetry to a discrete C_3 symmetry. The system spontaneously chooses one out of three allowed values of ϕ_+ and thereby breaks lattice rotational symmetry and becomes a nematic superconductor. Note that one of the states has $\phi_+ = 0$ and, hence, $\gamma = \pi/4$. For this state, the magnitudes of Δ_{E_1} and Δ_{E_2} are equal, only the relative angle $2\phi_-$ varies with Δ_{A_2}. However, the two E components of the gap are not equal in any given patch, as one gets multiplied by $\cos(4\theta_i + 3\pi/4)$, and the other by $\sin(4\theta_i + 3\pi/4)$, where, we remind, θ_i specify the directions towards VH points. For the other two solutions ($\phi_+ = \pm 2\pi/3$), we verified that the E components of the gap are the same as for the first solution if we rotate θ_i by $\pm\pi/3$. For $\delta^2 > 2\beta_2\gamma_2$, the ϕ_+-dependent term in the free energy Eq. (47) changes sign. In this case, another solution, with ϕ_- approximately $\pm 3\pi/4$ for $\Delta_{A_2} \ll \Delta_E$, becomes energetically favorable.

We also note that (i) the prefactor for the term quadratic in Δ_{A_2} in Eq. (47) is negative, i.e., for nonzero δ the transition temperature into the coexistence state is larger than the original $T_c^{A_2}$, where α_2 in Eq. (35) changes sign and (ii) the free energy (47) has a term proportional to $\Delta_{A_2}^3$. This term renders the transition between the pure E_2 state and the coexistence state first order.

We consider next the situation near the right boundary of the coexistence phase, where $\Delta_E \ll \Delta_{A_2}$. Let us assume for definiteness that without the δ term, $\phi_- = \pi/2$ and $\phi_+ = 0$ ($\Delta_{E_1} = i\cos\gamma$, $\Delta_{E_-} = -i\sin\gamma$), cf. Eq. (43). When δ is nonzero, we expand $\phi_- = \pi/2 + \varepsilon_-$ and $\phi_+ = 0 + \varepsilon_+$. Minimizing with respect to $\varepsilon_\pm$, we obtain

$$\begin{aligned} \varepsilon_+ &= \frac{\delta}{8\gamma_2}\frac{\Delta_E}{\Delta_{A_2}}\frac{\sin\gamma - \cos\gamma}{\sin\gamma\cos\gamma} \\ \varepsilon_- &= \frac{\delta}{4\gamma_2}\frac{\Delta_E}{\Delta_{A_2}}(\cos 3\gamma - \sin 3\gamma), \end{aligned} \tag{48}$$

and at the minimum

$$\mathcal{F}_{12p} = 2\alpha_1\Delta_E^2 + \alpha_2\Delta_{A_2}^2 + \left(\beta_1 + \beta_2 - \frac{\delta^2}{2\gamma_2}\right)\Delta_E^4 + \beta_3\Delta_{A_2}^4 + (\gamma_1 - 2\gamma_2)\Delta_E^2\Delta_{A_2}^2 + \frac{\beta_2\delta^2(\sin(6\gamma)-1)\Delta_E^6}{4\gamma_2^2\Delta_{A_2}^2}. \tag{49}$$

Contrary to the previous case, there is no $U(1)$ breaking term at order $O(\delta)$. However, such a term appears at order δ^2 with the structure $\delta^2 \sin 6\gamma$. Minimizing with respect to γ, we obtain $\gamma = \pi/4 + \pi n/3$, where $n = 0, \ldots, 5$ is an integer. We observe that now we have six solutions for γ within a 2π interval. One can verify that out of these six solutions, three are time-reversal partners of the other three, i.e., time-reversal symmetry is broken. One can understand this on physical grounds, because once the phase difference $2\phi_-$ between Δ_{E_1} and Δ_{E_2} becomes different from π, ϕ_- and $-\phi_-$ describe nonidentical gap configurations, hence under time reversal the system transforms into a physically different state. The remaining three solutions transform into each other under elements of C_3, i.e., the order parameter manifold is $U(1) \times C_3 \times Z_2$, the same that we obtained near the left boundary of the coexistence phase. Note that in Eq. (49) the correction to α_1 vanishes, and there is no Δ_E^3 term. As a consequence, the transition from the pure A_2 state into the coexistence state is second order as long as $4(\beta_1 + \beta_2 - \frac{\delta^2}{2\gamma_2})\beta_3 > (\gamma_1 - 2\gamma_2)^2$ (see Refs. [93–95]).

We verified that near the left boundary of the coexistence state, ϕ_- increases with Δ_{A_2} [cf. Eq. (46)], and near the right boundary ϕ_- decreases as Δ_E increases [cf. Eq. (48)], i.e., Δ_{E_1} and Δ_{E_2} rotate towards each other. This strongly suggests that the gap structure in the coexistence state evolves continuously for small but nonzero δ. We solved numerically for the gap at arbitrary ratio of Δ_{A_2}/Δ_E and found that this is indeed the case if $\delta^2 < 2\beta_2\gamma_2$. Specifically, for the "symmetric" state with $\phi_+ = 0$ and $\gamma = \pi/4$, we found a continuous change of ϕ_- inside the coexistence phase from $\phi_- \sim \pi/4$ for $\Delta_{A_2} \ll \Delta_E$ to $\phi_- \simeq \pi/2$ for $\Delta_{A_2} \gg \Delta_E$. We show the phase diagram in Fig. 1 along with the structure of the pure and coexistence states.

3. The case of large δ

We now show that a new state emerges at $\delta^2 > 2\beta_2\gamma_2$, which breaks C_3 symmetry but preserves time-reversal symmetry. To see this, we look again at the solutions close to the left and right boundaries. We found before that one of the solutions from the C_3 manifold is a symmetric one: $\phi_+ = 0$ and $\gamma = \pi/4$, i.e., $|\Delta_{E_1}| = |\Delta_{E_2}|$. Let us keep these values of ϕ_+ and γ but not assume that Δ_{A_2}/Δ_E is small and treat ϕ_- as parameter. We will use this as an ansatz for the ground state for larger δ and then verify that it is a stable minimum.

Substituting into Eq. (35), we obtain

$$\mathcal{F}_{12p} = 2\alpha_1\Delta_E^2 + \alpha_2\Delta_{A_2}^2 + 4\beta_1\Delta_E^4 + \beta_3\Delta_{A_2}^4 + 2\gamma_1\Delta_E^2\Delta_{A_2}^2 + \cos(2\phi_-)\big(2\gamma_2\Delta_E^2\Delta_{A_2}^2 + \beta_2\Delta_E^4 + 2\sqrt{2}\delta\Delta_E^3\Delta_{A_2}\cos(\phi_-)\big). \tag{50}$$

One can check that at large enough δ, the free energy has the smallest value when $\phi_- = \pm\pi$. For this ϕ_-, Eq. (50) reduces to

$$\mathcal{F} = 2\alpha_1\Delta_E^2 + \alpha_2\Delta_{A_2}^2 + (4\beta_1 + \beta_2)\Delta_E^4 + \beta_3\Delta_{A_2}^4 + 2(\gamma_1 + \gamma_2)\Delta_E^2\Delta_{A_2}^2 - 2\sqrt{2}\delta\Delta_E^3\Delta_{A_2}. \tag{51}$$

In such a state the phase of the two E components of the gap is opposite to the phase of the A_2 component, i.e., all three gap components, viewed as vectors, are directed along the same axis. Such a state preserves Z_2 time-reversal symmetry.

Rotational C_3 symmetry requires that there must be two other states with the same energy. In total, we find

$$\begin{aligned} &\phi_+ = 0 \quad \gamma = \pi/4 \quad \phi_- = \pm\pi \\ &\phi_+ = \pi/2 \quad \gamma = 5\pi/12 \quad \phi_- = \pi/2 \\ &\phi_+ = \pi/2 \quad \gamma = \pi/12 \quad \phi_- = -\pi/2. \end{aligned} \tag{52}$$

We now analyze where this "collinear" state is located in the phase diagram. For this we assume that it is present for some Δ_{A_2} and Δ_E and check its stability. For definiteness we choose the "symmetric" state with $\phi_+ = 0$, $\phi_- = \pi$, $\gamma = \pi/4$ and vary the angles by $\phi_- = \pi + \varepsilon_-$, $\phi_+ = \varepsilon_+$ and $\gamma = \pi/4 + \varepsilon_\gamma$. Substituting this into the free energy, we obtain to second order in ε_i

$$\begin{aligned} \mathcal{F}_{12p} = {} & 2\alpha_1\Delta_E^2 + \alpha_2\Delta_{A_2}^2 + (4\beta_1 + \beta_2)\Delta_E^4 + \beta_3\Delta_{A_2}^4 \\ & + 2(\gamma_1 + \gamma_2)\Delta_E^2\Delta_{A_2}^2 - 2\sqrt{2}\delta\Delta_E^3\Delta_{A_2} \\ & + \left[5\sqrt{2}\delta\Delta_E^3\Delta_{A_2} - 4\gamma_2\Delta_E^2\Delta_{A_2}^2 - 4\beta_2\Delta_E^4\right]\varepsilon_-^2 \\ & + 9\sqrt{2}\delta\Delta_{A_2}\Delta_E^3\varepsilon_\gamma^2 + \left[\sqrt{2}\delta\Delta_E^3\Delta_{A_2} - 4\gamma_2\Delta_E^2\Delta_{A_2}^2\right]\varepsilon_+^2. \end{aligned} \tag{53}$$

The stability conditions are then

$$\begin{aligned} &\sqrt{2}\delta\Delta_E^3\Delta_{A_2} - 4\gamma_2\Delta_E^2\Delta_{A_2}^2 \geqslant 0 \\ &5\sqrt{2}\delta\Delta_E^3\Delta_{A_2} - 4\gamma_2\Delta_E^2\Delta_{A_2}^2 - 4\beta_2\Delta_E^4 \geqslant 0. \end{aligned} \tag{54}$$

These conditions set the boundaries of the collinear phase at

$$\begin{aligned} \sqrt{2}\frac{5\delta + \sqrt{25\delta^2 - 32\beta_2\gamma_2}}{8\beta_2}\Delta_{A_2} &\geqslant \Delta_E \\ &\geqslant \sqrt{2}\frac{5\delta - \sqrt{25\delta^2 - 32\beta_2\gamma_2}}{8\beta_2}\Delta_{A_2} \end{aligned} \tag{55}$$

and

$$\Delta_E \geqslant \frac{4\gamma_2}{\sqrt{2}\delta}\Delta_{A_2}. \tag{56}$$

The first boundary is where fluctuations near $\phi_- = \pi$ become unstable, the second is where fluctuations near $\phi_+ = 0$ become unstable. Fluctuations of γ do not give an additional constraint. Combining these two conditions, we obtain that the phase with unbroken time-reversal symmetry exists once δ^2 exceeds $2\beta_2\gamma_2$ (we need $\sqrt{2}[5\delta + \sqrt{25\delta^2 - 32\beta_2\gamma_2}]/8\beta_2 \geqslant 4\gamma_2/\sqrt{2}\delta$). It starts as a line in the phase diagram at $\delta^2 = 2\beta_2\gamma_2$ and expands into the coexistence phase for larger δ. We show the phase diagram at large δ in Fig. 1 along with the states from the C_3 manifold inside the collinear phase, and in Fig. 12 we present the plots of the total gap function

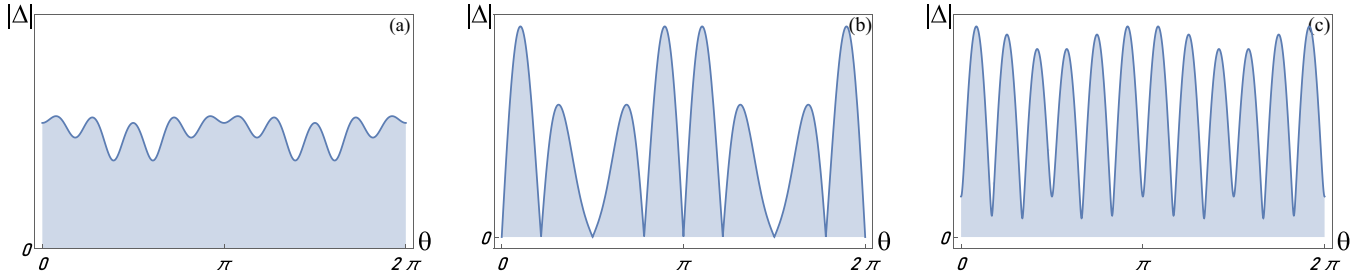

FIG. 12. The magnitude of the total gap function $\Delta^{SC}_{12p} = \Delta_{A_2}\mathbf{\Delta}^{A_2}_{12p} + \Delta_{E_1}\mathbf{\Delta}^{E_1}_{12p} + \Delta_{E_2}\mathbf{\Delta}^{E_2}_{12p}$ along the Fermi surface, when $\mathbf{\Delta}^{A_2}_{12p}$, $\mathbf{\Delta}^{E_1}_{12p}$, and $\mathbf{\Delta}^{E_2}_{12p}$ are viewed as functions of continuous θ rather than of θ_i at VH points. The three panels correspond to three coexistence states in the right panel of Fig. 1. We have chosen the symmetric state with $|\Delta_{E_1}| = |\Delta_{E_2}|$ (one of the states in C_3 manifold). Panel (b) is for the "collinear" state in the middle of the right panel of Fig. 1, and panels (a) and (c) are for the states to the left and to the right of the collinear state, respectively. We used $\Delta_{A_2}/\Delta_E = 0.2$, $\phi_- = 0.86$ in panel (a), $\Delta_{A_2}/\Delta_E = 0.71$ in panel (b), and $\Delta_{A_2}/\Delta_E = 6.6$, $\phi_- = 1.26$ in panel (c). The gap functions in panels (a) and (c) are complex numbers, and $|\Delta^{SC}_{12p}|$ has no nodes. The gap function in the collinear phase is real and has nodes, because $\mathbf{\Delta}^{E_1}_{12p}$, $\mathbf{\Delta}^{E_2}_{12p}$, and $\mathbf{\Delta}^{A_2}_{12p}$ have nodes (see Fig. 9). The gap structure in the left panel of Fig. 1 is the same as in panels (a) and (c).

$\Delta^{SC}_{12p} = \Delta_{A_2}\mathbf{\Delta}^{A_2}_{12p} + \Delta_{E_1}\mathbf{\Delta}^{E_1}_{12p} + \Delta_{E_2}\mathbf{\Delta}^{E_2}_{12p}$ for the three regions within the coexistence phase in the right panel of Fig. 1.

The condition $\delta^2 \geqslant 2\beta_2\gamma_2$ coincides with the condition that ϕ_- near the left boundary of the coexistence phase jumps from $\pi/4$ to $3\pi/4$. It then further increases with Δ_{A_2} and reaches π at the left boundary of the state with unbroken time-reversal symmetry. The evolution of the gap between the right boundary of the coexistence state and the collinear phase is more involved and we refrain from discussing it in detail. We note in passing that there is a certain analogy between the phase diagram and excitations in our case and for a 2D Heisenberg antiferromagnet in a magnetic field, whose phase diagram also contains an intermediate up-up-down phase with collinear ordering of spins in the three sublattices [96].

V. GAP STRUCTURE ALONG THE FULL FERMI SURFACE AND EXPERIMENTAL CONSEQUENCES

The gap structure along the full Fermi surface is shown in the three panels (a)–(c) in Fig. 12 for the three regions of the phase diagram in the right panel of Fig. 1 [the gap structure for the phase diagram in the left panel of Fig. 1 is the same but without middle panel (b)]. The gap function in panel (b) is for a SC state which preserves time-reversal symmetry and has nodes. The variation of this gap function with the angle θ along the Fermi surface is

$$\Delta(\theta) = \Delta_{A_2}\left(\sin 6\theta + \frac{\Delta_E}{\Delta_{A_2}}\sqrt{2}\sin 4\theta\right). \tag{57}$$

The number of nodes depends on the ratio Δ_E/Δ_{A_2}: For $\Delta_E/\Delta_{A_2} \lesssim 3/(2\sqrt{2})$ there are twelve nodes; for $\Delta_E/\Delta_{A_2} \gtrsim 3/(2\sqrt{2})$ the number of nodes is reduced to eight. The positions of four nodes are protected by time-reversal symmetry and are fixed at $\theta = 0, \pi/2, \pi, 3\pi/2$ (at these points both $\sin 6\theta$ and $\sin 4\theta$ components vanish). The location of the other nodal points depends on the ratio Δ_E/Δ_{A_2}.

The gap functions in panels (a) and (c) are for the states with broken time-reversal symmetry. These gap functions are nodeless by obvious reasons. They can be parameterized by

$$\Delta(\theta) = \Delta_{A_2}\Bigg[\sin 6\theta - \frac{1}{\sqrt{2}}\frac{\Delta_E}{\Delta_{A_2}}e^{i\phi_+}(\cos\phi_-[\cos(4\theta-\gamma) + \sin(4\theta-\gamma)] + i\sin\phi_-[\cos(4\theta+\gamma) + \sin(4\theta+\gamma)])\Bigg], \tag{58}$$

where ϕ_+, ϕ_- and γ evolve as functions of the ratio Δ_E/Δ_{A_2} [see Eqs. (46) and (48)]. The magnitude of the angle variation of $\Delta(\theta)$ depends on the ratio Δ_{A_2}/Δ_E and is larger in panel (c) (i.e., for the state at a larger α_T in the right panel of Fig. 1).

The gap structures, presented in Fig. 12, can be probed experimentally, by, e.g., QPI analysis of STM data and ARPES experiments. The states with and without nodes can also be distinguished by other techniques, e.g., by measuring the flux penetration depth. The ratio of Δ_{A_2} and Δ_E likely can be varied by, e.g., changing the twist angle or adding uniform strain, which changes the degree of the nonlocality of the interactions and hence affects our parameter α_T in Fig. 1. A discrete C_3 symmetry breaking was reported in Refs. [48,68] and motivated our study. It can also be detected in STM studies and in angle-resolved photoemission spectroscopy with nanoscale resolution [97]. A time-reversal symmetry breaking can be detected via a broad range of probes [98], including measurements of Kerr rotation [99] and zero-field muon-spin relaxation, which detects weak internal magnetic fields produced by spontaneous currents, generated around impurities by time-reversal breaking superconducting order [100–103]. Domain walls in such superconductors have magnetic signatures that could be detected in scanning SQUID and scanning Hall probe microscope measurements [104]. It was also proposed [105] that a nematic superconductor possesses topological skyrmions (bound states of two spatially separated half-quantum vortices), which can be detected by STM. On a qualitative level, a high T_c/T_F ratio, observed in magic-angle twisted bilayer graphene [1], is more consistent with the existence of attractive pairing interactions at the bare level rather than with Kohn-Luttinger scenario, in which the

attraction develops at second order in the interaction and is likely much weaker.

VI. CONCLUSIONS

In this paper we performed a comprehensive analysis of superconductivity near VH filling in twisted bilayer graphene (TBG) within an itinerant approach. The key motivation for our study has been the recent experimental finding [19,48,68] that the superconducting order in hole-doped TBG near $n = -2$ breaks C_3 lattice rotational symmetry, i.e., the SC state is also nematic.

We used as an input the effective tight-binding Hamiltonian for the moiré superlattice, which describes flat bands [14,61]. We argued that there are at least two VH fillings, one for hole doping, the other for electron doping. At VH filling for electron doping, there are six VH points, located along high symmetry directions in the Brillouin zone but away from the zone boundary. At VH filling for hole doping, there are twelve VH points. They are symmetry related, but each is located away from symmetry directions and the zone boundary. We derived effective six-patch and twelve-patch models for fermions near VH points and projected the interactions into the pairing channel. For the six-patch model, there are two symmetry-allowed pairing interactions in the spin-singlet channel. For the twelve-patch model this number is five. We obtained the values of the interactions by matching the patch models with the microscopic model of Kang and Vafek [13], which contains both local (Hubbard) and nonlocal interactions. The relative strength of the nonlocal interaction is measured by the parameter α_T, which was estimated to be around 0.23. We argued that for this α_T, the nonlocal interactions give rise to attraction in certain channels already at the "bare" level, i.e., without including corrections to the pairing interaction from the particle-hole channel. In other words, the reconstruction of the band structure due to the twist and projection onto the nearly flat bands leads to attractive pairing interactions in TBG. The attraction exists for both spin-singlet and spin-triplet channels. We concentrate on the first because experiments on TBG point to spin-singlet pairing [1].

The symmetry of the superconducting order parameter can be classified based on the irreducible representations of the lattice rotation symmetry group D_3. They include two one-dimensional representations, A_1 and A_2, and one two-dimensional representation, E. Each representation contains an infinite set of different eigenfunctions, but most become indistinguishable within patch models. For the six-patch model, we found that the relevant eigenfunctions are a constant (s wave) from A_1 and d-wave-like $(\cos 2\theta_i, \sin 2\theta_i)$ from E, where θ_i set the directions towards six VH points. We found that the interaction in the E channel is attractive and gives rise to $d \pm id$ SC order. It breaks time-reversal symmetry but preserves C_3 lattice rotational symmetry. This agrees with earlier results for the six-patch model [28,34] and with earlier studies of single-layer graphene around VH filling [46,47].

For the twelve-patch model, we found four different pairing channels: one in A_1, with a constant eigenfunction, one in A_2, with an eigenfunction changing signs between neighboring patches, and two in E with eigenfunctions $(\cos 2\theta_i, \sin 2\theta_i)$ and $(\cos 4\theta_i, \sin 4\theta_i)$. We found that A_2 and the 4θ E channel are attractive and that for realistic α_T the coupling constants in the two channels have near-equal magnitudes. We showed that pure A_2 order breaks only $U(1)$ phase symmetry, and pure E order is similar to that in the six-patch model, i.e., it breaks $U(1)$ and Z_2 time-reversal symmetry but preserves C_3.

Our key result is that in the coexistence state, where both E and A_2 order parameters are nonzero, C_3 symmetry is broken. We argued that this happens due to two reasons: (i) conventional biquadratic couplings between E and A_2 order parameters do not specify the coexistence state, and the order parameter manifold has an extra $U(1)$ symmetry, in addition to the $U(1)$ total phase symmetry, and (ii) the Landau free energy to quartic order contains a symmetry allowed term, which is linear in Δ_{A_2} and qubic in $\Delta_{E_{1,2}}$. This term breaks the extra $U(1)$ symmetry down to threefold C_3. The system spontaneously chooses one of three equivalent states from C_3 manifold and by doing this breaks C_3. As a result, the coexistence state turns out to be a nematic superconductor. We found two phases with broken C_3. In one, time-reversal symmetry is also spontaneously broken. In the other, it is preserved.

Our results present a scenario for the breaking of threefold lattice rotation symmetry in the superconducting state of hole-doped TBG near $n = -2$, where nematic superconductivity has been observed [19,48,68]. We also consider it as a generic, symmetry-based mechanism how a superconductor can break lattice rotational symmetry. We also emphasize that although in our scenario the nematic long-range order emerges only in the coexistence superconducting phase, nematic order generally survives in some range outside the coexistence phase, and nematic fluctuations are strong in the whole region where the pairing susceptibility is enhanced in both E and A_2 channels.

ACKNOWLEDGMENTS

We thank E. Andrei, M. Christensen, R. Fernandes, L. Fu, D. Goldhaber-Gordon, P. Jarillo-Herrero, J. Kang, A. Klein, L. Levitov, M. Navarro Gastiasoro, J. Schmalian, D. Shaffer, O. Vafek, J. Venderbos, and A. Vishwanath for fruitful discussions. The work was supported by US Department of Energy, Office of Science, Basic Energy Sciences, under Award No. DE-SC0014402. A.V.C. is thankful to Aspen Center for Physics (ACP) for hospitality during the completion of this work. ACP is supported by NSF Grant No. PHY-1607611. L.C. acknowledges support by the Humboldt foundation.

[1] Y. Cao, V. Fatemi, S. Fang, K. Watanabe, T. Taniguchi, E. Kaxiras, and P. Jarillo-Herrero, Nature (London) **556**, 43 (2018).

[2] Y. Cao, V. Fatemi, A. Demir, S. Fang, S. L. Tomarken, J. Y. Luo, J. D. Sanchez-Yamagishi, K. Watanabe, T. Taniguchi, E. Kaxiras *et al.*, Nature (London) **556**, 80 (2018).

[3] M. Yankowitz, S. Chen, H. Polshyn, Y. Zhang, K. Watanabe, T. Taniguchi, D. Graf, A. F. Young, and C. R. Dean, Science **363**, 1059 (2019).

[4] X. Lu, P. Stepanov, W. Yang, M. Xie, M. A. Aamir, I. Das, C. Urgell, K. Watanabe, T. Taniguchi, G. Zhang *et al.*, Nature (London) **574**, 653 (2019).

[5] Y. Cao, D. Rodan-Legrain, O. Rubies-Bigorda, J. M. Park, K. Watanabe, T. Taniguchi, and P. Jarillo-Herrero, Nature (London) (2020), doi: 10.1038/s41586-020-2260-6.

[6] X. Liu, Z. Hao, E. Khalaf, J. Y. Lee, K. Watanabe, T. Taniguchi, A. Vishwanath, and P. Kim, arXiv:1903.08130.

[7] C. Shen, Y. Chu, Q. S. Wu, N. Li, S. Wang, Y. Zhao, J. Tang, J. Liu, J. Tian, K. Watanabe *et al.*, Nat. Phys. **16**, 520 (2020).

[8] G. Chen, L. Jiang, S. Wu, B. Lyu, H. Li, B. L. Chittari, K. Watanabe, T. Taniguchi, Z. Shi, J. Jung, Y. Zhang, and F. Wang, Nat. Phys. **15**, 237 (2019).

[9] G. Chen, A. L. Sharpe, P. Gallagher, I. T. Rosen, E. J. Fox, L. Jiang, B. Lyu, H. Li, K. Watanabe, T. Taniguchi, J. Jung, Z. Shi, D. Goldhaber-Gordon, Y. Zhang, and F. Wang, Nature (London) **572**, 215 (2019).

[10] E. Suárez Morell, J. D. Correa, P. Vargas, M. Pacheco, and Z. Barticevic, Phys. Rev. B **82**, 121407(R) (2010).

[11] R. Bistritzer and A. H. MacDonald, Proc. Natl. Acad. Sci. **108**, 12233 (2011).

[12] H. C. Po, L. Zou, A. Vishwanath, and T. Senthil, Phys. Rev. X **8**, 031089 (2018).

[13] J. Kang and O. Vafek, Phys. Rev. Lett. **122**, 246401 (2019).

[14] M. Koshino, N. F. Q. Yuan, T. Koretsune, M. Ochi, K. Kuroki, and L. Fu, Phys. Rev. X **8**, 031087 (2018).

[15] K. Seo, V. N. Kotov, and B. Uchoa, Phys. Rev. Lett. **122**, 246402 (2019).

[16] F. Wu, E. Hwang, and S. Das Sarma, Phys. Rev. B **99**, 165112 (2019).

[17] F. Wu, A. H. MacDonald, and I. Martin, Phys. Rev. Lett. **121**, 257001 (2018).

[18] T. M. R. Wolf, J. L. Lado, G. Blatter, and O. Zilberberg, Phys. Rev. Lett. **123**, 096802 (2019).

[19] A. Kerelsky, L. J. McGilly, D. M. Kennes, L. Xian, M. Yankowitz, S. Chen, K. Watanabe, T. Taniguchi, J. Hone, C. Dean, A. Rubio, and A. N. Pasupathy, Nature (London) **572**, 95 (2019).

[20] Y. Kim, P. Herlinger, P. Moon, M. Koshino, T. Taniguchi, K. Watanabe, and J. H. Smet, Nano Lett. **16**, 5053 (2016).

[21] G. Li, A. Luican, J. M. B. Lopes dos Santos, A. H. Castro Neto, A. Reina, J. Kong, and E. Y. Andrei, Nat. Phys. **6**, 109 (2010).

[22] K. L. Hur and T. M. Rice, Ann. Phys. **324**, 1452 (2009), July 2009 Special Issue.

[23] R. Samajdar and M. S. Scheurer, arXiv:2001.07716.

[24] B. Lian, Z. Wang, and B. A. Bernevig, Phys. Rev. Lett. **122**, 257002 (2019).

[25] Y. W. Choi and H. J. Choi, Phys. Rev. B **98**, 241412(R) (2018).

[26] T. J. Peltonen, R. Ojajärvi, and T. T. Heikkilä, Phys. Rev. B **98**, 220504(R) (2018).

[27] J. W. F. Venderbos and R. M. Fernandes, Phys. Rev. B **98**, 245103 (2018).

[28] H. Isobe, N. F. Q. Yuan, and L. Fu, Phys. Rev. X **8**, 041041 (2018).

[29] S. Ray, J. Jung, and T. Das, Phys. Rev. B **99**, 134515 (2019).

[30] J. González and T. Stauber, Phys. Rev. Lett. **122**, 026801 (2019).

[31] Y. Sherkunov and J. J. Betouras, Phys. Rev. B **98**, 205151 (2018).

[32] Y.-Z. You and A. Vishwanath, npj Quantum Materials **4**, 1 (2019).

[33] Y.-P. Lin and R. M. Nandkishore, Phys. Rev. B **98**, 214521 (2018).

[34] Y.-P. Lin and R. M. Nandkishore, Phys. Rev. B **100**, 085136 (2019).

[35] W. Chen, Y. Chu, T. Huang, and T. Ma, Phys. Rev. B **101**, 155413 (2020).

[36] X.-C. Wu, K. A. Pawlak, C.-M. Jian, and C. Xu, arXiv:1805.06906.

[37] J. F. Dodaro, S. A. Kivelson, Y. Schattner, X. Q. Sun, and C. Wang, Phys. Rev. B **98**, 075154 (2018).

[38] C. Xu and L. Balents, Phys. Rev. Lett. **121**, 087001 (2018).

[39] M. Fidrysiak, M. Zegrodnik, and J. Spałek, Phys. Rev. B **98**, 085436 (2018).

[40] E. Laksono, J. N. Leaw, A. Reaves, M. Singh, X. Wang, S. Adam, and X. Gu, Solid State Commun. **282**, 38 (2018).

[41] C.-C. Liu, L.-D. Zhang, W.-Q. Chen, and F. Yang, Phys. Rev. Lett. **121**, 217001 (2018).

[42] Y. Su and S.-Z. Lin, Phys. Rev. B **98**, 195101 (2018).

[43] Z. Liu, Y. Li, and Y.-F. Yang, Chin. Phys. B **28**, 077103 (2019).

[44] D. M. Kennes, J. Lischner, and C. Karrasch, Phys. Rev. B **98**, 241407(R) (2018).

[45] L. Classen, C. Honerkamp, and M. M. Scherer, Phys. Rev. B **99**, 195120 (2019).

[46] R. Nandkishore, L. Levitov, and A. Chubukov, Nat. Phys. **8**, 158 (2012).

[47] M. L. Kiesel, C. Platt, W. Hanke, D. A. Abanin, and R. Thomale, Phys. Rev. B **86**, 020507(R) (2012).

[48] Y. Cao, D. Rodan-Legrain, J. M. Park, F. N. Yuan, K. Watanabe, T. Taniguchi, R. M. Fernandes, L. Fu, and P. Jarillo-Herrero, arXiv:2004.04148.

[49] Y. S. Kushnirenko, D. V. Evtushinsky, T. K. Kim, I. V. Morozov, L. Harnagea, S. Wurmehl, S. Aswartham, A. V. Chubukov, and S. V. Borisenko, arXiv:1810.04446.

[50] Y. S. Hor, A. J. Williams, J. G. Checkelsky, P. Roushan, J. Seo, Q. Xu, H. W. Zandbergen, A. Yazdani, N. P. Ong, and R. J. Cava, Phys. Rev. Lett. **104**, 057001 (2010).

[51] L. Fu and E. Berg, Phys. Rev. Lett. **105**, 097001 (2010).

[52] L. Fu, Phys. Rev. B **90**, 100509(R) (2014).

[53] K. Matano, M. Kriener, K. Segawa, Y. Ando, and G.-q. Zheng, Nat. Phys. **12**, 852 (2016).

[54] J. W. F. Venderbos, V. Kozii, and L. Fu, Phys. Rev. B **94**, 180504(R) (2016).

[55] S. Yonezawa, K. Tajiri, S. Nakata, Y. Nagai, Z. Wang, K. Segawa, Y. Ando, and Y. Maeno, Nat. Phys. **13**, 123 (2017).

[56] M. Hecker and J. Schmalian, npj Quantum Materials **3**, 26 (2018).

[57] C.-w. Cho, J. Shen, J. Lyu, S. H. Lee, Y. San Hor, M. Hecker, J. Schmalian, and R. Lortz, arXiv:1905.01702.

[58] Y. Jiang, X. Lai, K. Watanabe, T. Taniguchi, K. Haule, J. Mao, and E. Y. Andrei, Nature (London) **573**, 91 (2019).

[59] X. Wu, W. Hanke, M. Fink, M. Klett, and R. Thomale, Phys. Rev. B **101**, 134517 (2020).

[60] V. Kozii, H. Isobe, J. W. F. Venderbos, and L. Fu, Phys. Rev. B **99**, 144507 (2019).

[61] N. F. Q. Yuan and L. Fu, Phys. Rev. B **98**, 045103 (2018).
[62] M. S. Scheurer and R. Samajdar, arXiv:1906.03258.
[63] N. F. Q. Yuan, H. Isobe, and L. Fu, Nat. Commun. **10**, 5769 (2019).
[64] X. Wu, M. Fink, W. Hanke, R. Thomale, and D. Di Sante, Phys. Rev. B **100**, 041117(R) (2019).
[65] See Supplemental Material at http://link.aps.org/supplemental/10.1103/PhysRevB.101.224513 for details of the derivations.
[66] J. Kang and O. Vafek, Phys. Rev. X **8**, 031088 (2018).
[67] M. Hamermesh, *Group Theory and Its Application to Physical Problems* (Addison-Wesley, Reading, MA, 1964).
[68] P. Jarillo-Herrero, Talk at KITP Rapid Response Workshop.
[69] J. M. B. Lopes dos Santos, N. M. R. Peres, and A. H. Castro Neto, Phys. Rev. Lett. **99**, 256802 (2007).
[70] E. J. Mele, Phys. Rev. B **81**, 161405(R) (2010).
[71] E. J. Mele, Phys. Rev. B **84**, 235439 (2011).
[72] J. M. B. Lopes dos Santos, N. M. R. Peres, and A. H. Castro Neto, Phys. Rev. B **86**, 155449 (2012).
[73] P. Moon and M. Koshino, Phys. Rev. B **85**, 195458 (2012).
[74] P. Moon and M. Koshino, Phys. Rev. B **87**, 205404 (2013).
[75] M. Koshino and P. Moon, J. Phys. Soc. Jpn. **84**, 121001 (2015).
[76] N. N. T. Nam and M. Koshino, Phys. Rev. B **96**, 075311 (2017).
[77] S. Shallcross, S. Sharma, E. Kandelaki, and O. A. Pankratov, Phys. Rev. B **81**, 165105 (2010).
[78] G. Trambly de Laissardière, D. Mayou, and L. Magaud, Nano Lett. **10**, 804 (2010).
[79] J. Jung, A. Raoux, Z. Qiao, and A. H. MacDonald, Phys. Rev. B **89**, 205414 (2014).
[80] S. Fang and E. Kaxiras, Phys. Rev. B **93**, 235153 (2016).
[81] H. C. Po, L. Zou, T. Senthil, and A. Vishwanath, Phys. Rev. B **99**, 195455 (2019).
[82] L. Zou, H. C. Po, A. Vishwanath, and T. Senthil, Phys. Rev. B **98**, 085435 (2018).
[83] G. Trambly de Laissardière, D. Mayou, and L. Magaud, Phys. Rev. B **86**, 125413 (2012).
[84] Y. Cao, J. Y. Luo, V. Fatemi, S. Fang, J. D. Sanchez-Yamagishi, K. Watanabe, T. Taniguchi, E. Kaxiras, and P. Jarillo-Herrero, Phys. Rev. Lett. **117**, 116804 (2016).
[85] H. Isobe and L. Fu, Phys. Rev. Research **1**, 033206 (2019).
[86] S. Maiti and A. V. Chubukov, AIP Conf. Proc. **1550**, 3 (2013).
[87] R. Shankar, Rev. Mod. Phys. **66**, 129 (1994).
[88] W. Metzner, M. Salmhofer, C. Honerkamp, V. Meden, and K. Schönhammer, Rev. Mod. Phys. **84**, 299 (2012).
[89] C. Platt, W. Hanke, and R. Thomale, Adv. Phys. **62**, 453 (2013).
[90] J. González, Phys. Rev. B **88**, 125434 (2013).
[91] M. Sigrist and K. Ueda, Rev. Mod. Phys. **63**, 239 (1991).
[92] B. Zinkl, M. H. Fischer, and M. Sigrist, Phys. Rev. B **100**, 014519 (2019).
[93] K.-S. Liu and M. E. Fisher, J. Low Temp. Phys. **10**, 655 (1973).
[94] P. Calabrese, A. Pelissetto, and E. Vicari, Phys. Rev. B **67**, 054505 (2003).
[95] A. Eichhorn, D. Mesterházy, and M. M. Scherer, Phys. Rev. E **88**, 042141 (2013).
[96] A. V. Chubukov and D. I. Golosov, J. Phys.: Condens. Matter **3**, 69 (1991).
[97] M. I. B. Utama, R. J. Koch, K. Lee, N. Leconte, H. Li, S. Zhao, L. Jiang, J. Zhu, K. Watanabe, T. Taniguchi, P. D. Ashby, A. Weber-Bargioni, A. Zettl, C. Jozwiak, J. Jung, E. Rotenberg, A. Bostwick, and F. Wang, arXiv:1912.00587.
[98] J. Carlström, J. Garaud, and E. Babaev, Phys. Rev. B **84**, 134518 (2011).
[99] A. Kapitulnik, Physica B: Condens. Matter **460**, 151 (2015), special Issue on Electronic Crystals (ECRYS-2014).
[100] Z. L. Mahyari, A. Cannell, C. Gomez, S. Tezok, A. Zelati, E. V. L. de Mello, J.-Q. Yan, D. G. Mandrus, and J. E. Sonier, Phys. Rev. B **89**, 020502(R) (2014).
[101] X. Hu and Z. Wang, Phys. Rev. B **85**, 064516 (2012).
[102] J. Garaud, M. Silaev, and E. Babaev, Physica C: Supercond. Appl. **533**, 63 (2017), ninth international conference on Vortex Matter in nanostructured Superconductors.
[103] S.-Z. Lin, S. Maiti, and A. Chubukov, Phys. Rev. B **94**, 064519 (2016).
[104] J. Garaud and E. Babaev, Phys. Rev. Lett. **112**, 017003 (2014).
[105] A. A. Zyuzin, J. Garaud, and E. Babaev, Phys. Rev. Lett. **119**, 167001 (2017).